Simulation and analysis of E-fields of dual-site tACS at various phase-lag values

Biomedical Signals & Systems

Bachelor Thesis - Faculty of Science & Technology

Student
Marieke Rona *(S2083922)*

Exam Committee
Msc. Ir. Silvana Huertas Penen - *Daily Supervisor*
Dr. Ir. Bettina C. Schwab - *Supervisor*
Dr. Maria C. Piastra - *Committee member*

Date:
December 15, 2022

UNIVERSITY OF TWENTE.

Abstract

tACS is a non-invasive stimulation technique where oscillating currents are applied to externally modulate cortical excitability and connectivity in the brain. While tACS seems to have promising results in altering oscillatory activity, there is a high variability of results between studies and subjects. There is a need for understanding the physiological mechanisms behind tACS. This study investigated changes in the tACS-induced electric field as a result of changing the size of stimulation ring electrodes and changing the phase-lag value between two cortices. A standard SimNIBS pipeline was used for finite element methods calculations, using Dirichlet and Neumann boundaries. A quasi-static regime is assumed.

In this study, we have found more information on how the electric field induced by tACS responds to different settings of stimulation. Firstly, the sizes of the center-surround ring electrodes were changed and simulated. A compromise for a high focality and high strength of the electric field was found in the ring electrode montage where (D_{circle}, $D_{inner-ring}$, $D_{outer-ring}$) = (25, 78, 100) mm. Next, the effect of a phase-lag value between the cortices was simulated for values of $\phi = 0$, $\phi = \pi$, $\phi = 1/2\pi$, and $\phi = 3/2\pi$. The strength of the induced electric field is dependent on the tACS current that is applied through the electrodes. Changes in the electric field distribution compared to the $\phi = 0$ stimulation, led to differences located below the stimulation electrodes. When the currents are of opposite polarity, there is also a difference present at the great longitudinal fissure. The direction of the electric field gradually changed from perpendicular to the cortex to a more parallel orientation to the cortex for all phase-lag simulations.

While we gained new insights, the results are limited by their generalizability. With more research, the generalizability of the results could be expanded and new insights could be made.

Table of Contents

1 Introduction

Transcranial electrical stimulation (tES) is a non-invasive stimulation technique where currents are applied to the scalp to alter brain function[1]. Studying the physiology of human cognition and the motor cortices has been difficult due to technological and ethical constraints[2]. tES techniques could be a solution, as they study physiology in a non-invasive manner. tES compromises a number of different techniques, transcranial alternating current stimulation (tACS) being one of them.

In tACS, oscillating electrical currents are applied to externally modulate cortical excitability and brain connectivity[3]. Since tACS can interfere with or enhance brain waves depending on the settings of stimulation, it has been studied as a means of intervention in different neurological and behavioral conditions and diseases[3, 4, 5]. For example, tACS can be effective in altering brain waves and oscillatory activity characteristics for motor dysfunctions associated with Parkinson's disease[5]. Furthermore, tACS has been proven effective in reducing auditory hallucinations in patients with schizophrenia[6]. While the results of tACS seem promising, there is a high variability of these results between studies and subjects[7].

There is a need for further studies to have an understanding of the physiological mechanisms behind tACS[8]. With a better understanding, the results of tACS can be predicted more accurately and variability between subjects can be decreased. The first step in understanding is analyzing how different stimulation parameters influence the tACS-induced electric field in the cortex. When there is an understanding of how we can influence the electric field with different parameters, we could predict and control the effects of tACS.

1.1 The mechanisms and effects of tACS

In tACS oscillating electrical currents are applied to the scalp to induce electric fields in the cortex. A large part of the applied current will be shunted by the scalp, not reaching the intended area for stimulation[9]. Thus, a weak alternating current reaches the brain. This current causes the membrane potential of cortical neurons to move towards hyper- or de-polarization, which increases the chance of an action potential being generated[4, 10].

tACS can be separated by the timing of its effects: the online effects (during the tACS stimulation) and the offline effects (after the tACS stimulation)[4]. The online effects are thought to be caused by the synchronization of brain oscillations to the applied tACS current[11]. The main physiological mechanisms that are hypothesized to be responsible for these online effects are entrainment and intrinsic endogenous resonance[12]. Entrainment is the phenomenon where brain oscillations will synchronize to the frequency of the tACS current.

While it would be helpful to study the online effects of tACS, this has proven to be difficult. The effects or tACS could be measured using EEG [13]. However, tACS stimulation causes hard-to-predict artifacts in the electric signal[14]. The strength of these artifacts is relatively high compared to the signals measured with EEG, making interpretation of results difficult[14, 15]. Since measuring the online effects is hard due to these artifacts, studying the offline effects of EEG has become the standard. While there are some studies on fMRI and MEG to investigate the effects of tACS in the brain, EEG seems the most logical complement[15]. EEG and MEG measurements reflect the electric activity of neuronal cells[16]. Thus, EEG and MEG study the direct effects of tACS, unlike fMRI. Furthermore, EEG and MEG have a relatively high temporal resolution compared to fMRI, making them a more suitable method of measurement[13]. In practice, EEG is used more than MEG since it is cheaper and easier to access[17].

High subject variability of offline tACS-induced effects can be caused by the lack of understanding of the physiological mechanisms[9]. Between studies, the settings of stimulation, such as the intensity of stimulation and the electrode montage, are changed[8]. More research on which physiological effects are behind tACS is needed, taking into consideration the different settings of stimulation.
The offline effects of tACS are suggested to be caused by both entrainment and spike-timing-dependent plasticity (STDP)[18]. There is a debate on whether the effects of entrainment outlast the time of stimulation and thus be observed when measuring offline effects [19]. STDP is thought to make changes in the synapses depending on the endogenous frequency of the neural networks. Plastic changes can occur, for example, if the frequency of tACS is matched to this endogenous frequency of the neural networks[20, 18]. Thus, STDP could cause synchronization or desynchronization of neuronal activity[2, 21].

1.2 Stimulation parameters of tACS

tACS can be expanded to have multiple sites of stimulation, e.g. dual-site tACS. In dual-site tACS, electrode montages are placed on two different brain regions, most commonly on two contralateral regions. Dual-site tACS is thought to be useful in modulating the phases of brain oscillations in two connected cortical areas[22].

There are different stimulation parameters that can be varied during tACS, e.g. the frequency of stimulation. Two of these stimulation parameters are the montage of the stimulation electrodes and the phase-lag between two regions of stimulation.

The electrode montage of tACS
The montage of stimulation electrodes in tACS can influence the effects that are induced[23]. Datta et al. (2008) tested a variety of different montages, e.g. distant-bipolar, adjacent-bipolar, tripolar, and (concentric) ring montages. The ring electrode montage (see Figure 1B) resulted in the highest focality of the electric field[24]. A stronger focalization of the electric field is associated with more consistent brain activity[23]. In the ring montage, the outer ring acts as a curved electrode and guides the current in the direction of the region of interest: the current moves from the center electrode to the outer ring electrode which acts as a boundary for the current. This principle explains the high focality of the electric field for the ring montage. In a classical montage (see Figure 1A), the expansion of the electric field is less focal, making it more difficult to target a certain brain area[23].

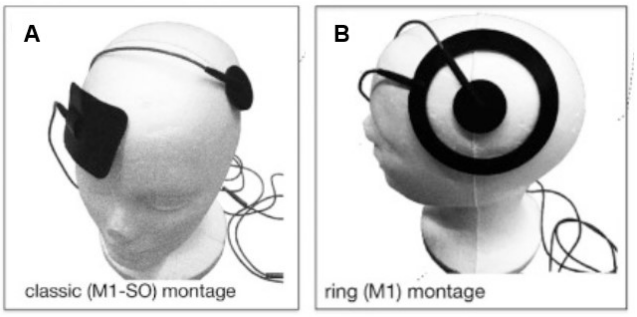

Figure 1: In Figure 1A, a classical tACS montage can be seen. In Figure 1B, a tACS ring montage can be seen. The ring montage is characterized by having a circular center electrode surrounded by a larger ring electrode. Figure from [23].

Studies have shown that changing the properties of electrodes could improve the focality of the electric field during tACS[9]. While a ring montage results in a relatively high focality of the electric field, it does so at the expense of having a decreased total current on the cortical surface[24]. Changing the sizes of the ring electrodes could be proven useful to find a compromise between having a high focality

and lower total current.

A phase-lag value of tACS
The phase between the different sites is important since the activity and connectivity of the brain could be altered depending on the value of the phase-lag[25]. Using different phase-lag values between two regions of the brain seems to induce effects that outlast the time of stimulation. Differences in connectivity changes were found between an in-phase stimulation ($\phi = 0$) and an anti-phase stimulation ($\phi = \pi$)[26]. It seems that neural activity can be influenced phase-specifically by the electric field.

tACS currents are most commonly applied as sinusoids, which in its most basic form looks like:

$$F = I_o sin(2\pi ft + \phi)$$

A phase-lag is a 'delay' in the applied sinusoid. The value of ϕ changes and thereby changes the offset of the current. When we speak of a phase-lag of $\phi = 0$, we mean that the offset of the current is the same in both stimulation sites. When we speak of a phase-lag of $\phi = \pi$, we mean that the offset for the current in one stimulation site is 0, while it is π in the other stimulation site (see Figure 2).

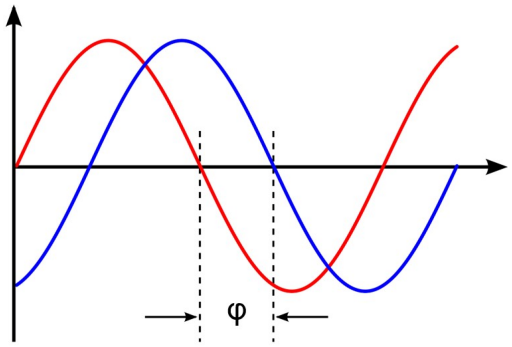

Figure 2: An example of what a phase-lag between the sinusoidal currents would look like. The ϕ indicates a delay in the offset of one of the currents. Figure adapted from [27].

1.3 tACS effects on the electric field

The electric current that passes through the stimulation electrodes generates an electric field. This electric field alters brain activity and connectivity. The electric field is influenced by the setting of stimulation parameters during tACS. To understand how the field is influenced by the settings of stimulation, its focality, strength, and direction can be used as a measurement.

The focality of the electric field is a measurement of how much the electric field diverges. A low focality means that the electric field is more widespread in the cortices, and thus that more brain areas could be modulated. In order to be able to find a causal relationship between the stimulation effect on the electric field and the modulation of specific brain areas or waves, it is important to limit the induced electric field to a region of interest[28].
In tACS, the 'dose' refers to the induced electric fields in the cortex[29]. Induced electric fields with a strength of 0.2 V/m are already expected to modulate neurons. However, an increased focality of the electric field is often accompanied by a decrease in the electric field strength[28]. It is important to analyze this strength-focality trade-off, to choose the most efficient tACS stimulation parameters.

Another measure related to the electric field is its direction. The direction of the applied current to the stimulated region of interest is thought to play an essential role in the effects of tACS[12]. In single neurons, the direction of the tACS current to the somatodendritic axis of the targeted neurons decides

if there is hyperpolarization, depolarization, or no polarization[30]. Thus, when the direction of the applied electric field changes, the properties of the resulting field in the cortex change as there might be a different subset of neurons that is stimulated[4, 25]. The direction of the applied current to the orientation of the targeted neurons can alter the effects of tACS significantly[30].

1.4 Quasi-static approximation and FEM for tACS simulation

SimNIBS and Matlab can be used to simulate tDCS, TMS, and tACS. The response of the electric field on different stimulation parameters during dual-site tACS can be simulated. The finite element method (FEM) and the quasi-static approximation are used to be able to do tACS simulations in SimNIBS using the tDCS pipeline (see Chapter 3.1 for an elaboration). How the quasi-static approximation and FEM can be applied in theory, will be discussed here.

Frequencies used in tACS are relatively low, meaning a quasi-static approximation can be made. We can assume a quasi-static approximation if [31]:

$$L/c \ll \tau$$

With L the diameter of the head, $\tau = 1/f$ the time of interest and $c = 1/\sqrt{\epsilon_0 \mu_0}$

For a frequency $F = 20$ Hz, the sphere of the head approximated with $L = 13$ cm, we get:

$$L/c \cong 4.310^{-10} \text{ s} \ll 0.05 \text{ s}$$

In this case, the quasi-static approximation can be made. This means that the temporal component and the spatial component can be seen as independent of one another. The temporal variation will only scale the electric field and does not change the distribution [32].

If a quasi-static regime can be assumed, the transcranial direct current stimulation (tDCS) SimNIBS pipeline can be used for tACS simulations. Based on the quasi-static approximation, the spatial component of the electric field can be calculated by solving Laplace's equation for the electrostatic potential φ [33, 31]:

$$\nabla \cdot (\sigma \nabla \varphi) = 0$$

The tDCS model can be regarded as a mixed boundary value problem[31]. The electrostatic potential ϕ at the location of the electrodes is determined by Dirichlet boundary conditions[33, 34]. The electrostatic potential at the rest of the surface of the head is determined by Neumann boundary conditions ($\nabla \varphi = 0$) since no current flows from the scalp to the air[35]. With these boundary conditions, FEM can be used to determine electric field E by numerical differentiation of φ [33]:

$$\mathbf{E} = -\nabla \varphi$$

In the case of tDCS/tACS simulations, electrodes are added to the head model. Therefore, the head model coordinate system is aligned with the coordinate system for the electrodes[36]. Then, the body of the electrodes are constructed by filling in tetrahedra. FEM can be used to calculate the electric field at each element of the head mesh. FEM is generally used to compute solutions of numerical model equations which are an approximation of the solution to the partial differential equations [37]. In this case, that means that FEM is used with linear basis functions. The FEM calculations result in an electric field at each element of the head mesh. The mesh is transformed into a cortical surface using interpolation, so that visualization is easier.

2 Aims of Research

In this study, we aim to investigate changes in the electric field as a result of changing the size of stimulation ring electrodes and changing the phase-lag value between two cortices, during dual-site tACS targeted to the primary motor cortices (M1). First, we will evaluate how different ring electrode sizes affect the electric field by measuring the focality in the cortex and the maximum and average strength of the electric field in the primary motor cortex. Next, we will study how phase-lag values of $\phi = 0$, $\phi = \pi$, $\phi = \frac{1}{2}\pi$, and $\phi = \frac{3}{2}\pi$ between cortices affect the electric field by measuring the focality in the cortex, the maximum and average strength, and the direction of the electric field. We will simulate the stimulations with different ring electrode sizes and phase-lag values in SimNIBS 2.3.6 and Matlab R2021B. Using the finite element method (FEM), calculated with SimNIBS, an accurate approximation of the electric fields in the human head is made. Since the frequencies used in tACS are relatively low, a quasi-static approximation can be made. The focality, the maximum and average strength, and the direction of the electric field in the primary motor cortices will be studied to evaluate the response of the electric field to the differences in stimulation parameters.

In summary, the aims of the study are:

- Simulate and evaluate different center-surround ring electrode configurations in tACS.
  - Analyse the focality of the induced electric field in the primary motor cortex for different ring electrode configurations;
  - Analyse the maximum and average field strength of the induced field in the primary motor cortex for different ring electrode configurations;
  - Give a recommendation on the best ring electrode montage based on the focality and maximum and average strength of the electric field in the simulations.
- Simulate and evaluate the effect of the phase-lag values $\phi = 0$, $\phi = \pi$, $\phi = \frac{1}{2}\pi$, and $\phi = \frac{3}{2}\pi$ applied between cortices in tACS.
  - Analyse the focality of the induced electric field in the primary motor cortex for different phase-lag values.
  - Analyse the maximum and average field strength of the induced field in the primary motor cortex for different phase-lag values.
  - Study the direction of the induced electric field in the primary motor cortex for different phase-lag values.
  - Compare the different induced electric fields in the primary motor cortices for different phase-lag values.

2.1 Relevance of results

There is a need for understanding the physiological mechanisms behind tACS to better predict its results. In this study, we will analyze the effect of different stimulation parameters (ring electrode sizes and phase-lags between cortices) on the properties of the electric field. We aim to better understand the induced electric field as a result of tACS. This is the first step in better understanding the mechanisms behind tACS.

The results of tACS could be predicted more accurately when the physiological mechanisms are better understood. It would help in determining the experimental design that is best suited for tACS. Neuroscientists could design an optimal tACS configuration, suited for stimulating specific brain oscillations. Furthermore, the modeling of the induced current could be adopted to predict effects for a specific patient[30].

3 Methods

As mentioned in Chapter 2, we aim to study the effect of different ring electrode montages and phase-lag values on the behavior of the electric field in tACS simulations. First, the different ring electrode montages are simulated. Based on these results, the best montage will be chosen as a compromise between a high field focality and a high strength of the electric field. Then, this montage is used for the simulation of tACS with different phase-lag values. This chapter will cover the methods of these experiments in more detail.

3.1 General experimental set-up

A standard SimNIBS software pipeline is used for the FEM simulation of tACS. This pipeline segments T1- and T2-weighted anatomical volumes into five tissue types. The finite element method (FEM) is used to accurately approach the electric field of the complex geometrical shape of the human head [33, 38]. FEM simulations were performed for the different center-surround ring electrode montages and phase-lag values using the ICBM125 MRI head model template[39, 40]. In all simulations, we used a center-surround ring electrode. The center-surround ring electrodes have an inside center electrode that is surrounded by an outer ring electrode (see Figure 1B). The inside electrodes were placed on the C3 and C4 EEG electrodes according to the 10/10 EEG system (see Figures 3 and 4), as they are the locations of the centers of M1 [41]. The thickness of the simulated electrodes (inner and outer) is 5mm in all simulations.

In this experiment, we simulate the application of tACS with a frequency of 20 Hz. In Chapter 1.4, we have shown that for this frequency a quasi-static approximation can be made. Therefore, we will use the SimNIBS tDCS pipeline to simulate tACS. We can approximate a tACS simulation with a current that is a set value, since the distribution of the electric field will not change, only the scaling. Thus, the tACS simulations are approximated by using a static regime. Since the current in our tACS simulations is applied as a sinusoid, we can take the value of this sinusoid at an arbitrary point in time, and take this as a current value.

Figure 3: The general set-up of the center-surround ring electrodes. The inside electrode of the rings is placed on C3 and C4 EEG electrode positions. The exact diameter of both the inside and outside electrodes will be varied in simulations.

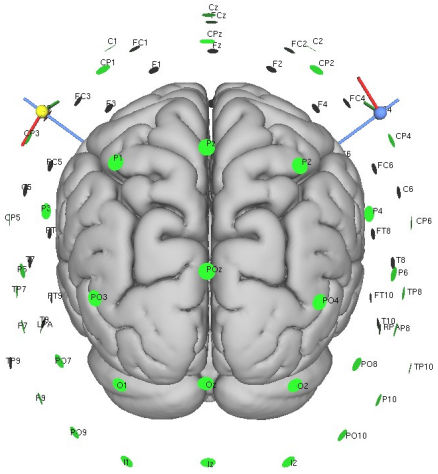

Figure 4: An overview of the different EEG electrode positions in the 10/10 EEG system. There is a yellow pinpoint indicating the location of C3 and a blue pinpoint indicating C4.

Analysis of the electric field was done in the region of interest (ROI): the primary motor cortex. The coordinates for the maximum activation likelihood estimation (ALE) value of M1 are taken as the center coordinates of our ROI [42]. For the left hemisphere, these coordinates are $peak_x$ = -37, $peak_y$

= -21, and $peak_z$ = 58. For the right hemisphere the coordinates are $peak_x$ = 37, $peak_y$ = -21, and $peak_z$ = 58 (see Figure 5). A sphere with a radius of 10 mm is 'visualized' around the center coordinates. When the average and maximum field strength are calculated, the electric field values that lie within this sphere are taken into consideration. The values of the electric field outside of this sphere are considered outside of the ROI, and thus will not be taken into account during analysis. For the calculations of the focality and the direction of the electric field, the fields in the entire cortex are taken into account.

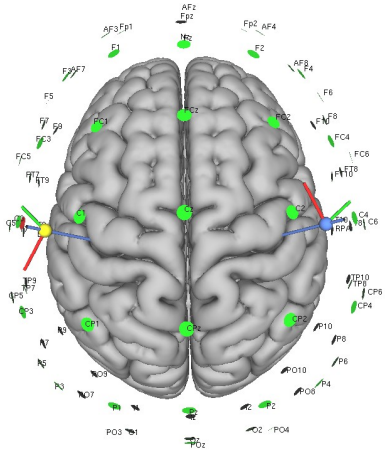

Figure 5: The center of our ROIs is indicated with a yellow and a blue pinpoint. In our analysis, the ROI is approximated as a sphere with a diameter of 10mm around this center.

3.2 Simulation of different ring electrode montages

We simulated different combinations of center-surround ring electrode montages. The diameter of the inside electrode (D_{circle}), the inner diameter of the outside electrode ($D_{inner-ring}$), and the outer diameter of the outside electrode ($D_{outer-ring}$) can be varied. The different ring electrode montages that were simulated can be found in Table 1. The different sizes of the electrodes were chosen based on commercial availability for tACS.
The induced electric fields for a phase-lag $\phi = 0$ and $\phi = \pi$ were compared in the maximum strength of the electric field in the ROI, and the focality in the gray matter. The maximum strength of the electric field in the ROI is measured as the 99.9^{th} percentile in V/m. The field focality is measured as the area of the gray matter that has a field with $\geq 75\%$ of the 99.9^{th} percentile, in mm^3.

3.3 Simulation of different phase-lag values

We simulated different phase-lag values with a ring electrode montage of (D_{circle}, $D_{inner-ring}$, $D_{outer-ring}$ = (25, 78, 100) mm. In the analysis of the effect of different ring electrode montages, the best ring configuration was chosen based on a compromise between a high electric field strength and a high focality of the electric field (see more in Chapter 4.1.1). In the analysis of the effect of phase-lag values, ring electrodes are used with $D_{circle} = 25$ mm, $D_{inner-ring} = 78$ mm, and $D_{outer-ring} = 100$ mm. The phase-lag between the two electrodes on the cortices is varied in the simulations. Phase-lag values of $\phi = 0, \phi = \frac{1}{2}\pi, \phi = \pi, \phi = \frac{3}{2}\pi$ are simulated and analyzed.

The induced electric fields in the cortex were compared in the maximum and average strength of the electric field in the ROI, and the focality in the gray matter. The strength and focality of the electric fields as a result of the different electrode sizes were analyzed in both in-phase and anti-phase. The maximum strength of the electric field in the ROI is measured as the 99.9^{th} percentile in V/m. The field focality is measured as the area of the gray matter that has a field with $\geq 75\%$ of the 99.9^{th} percentile,

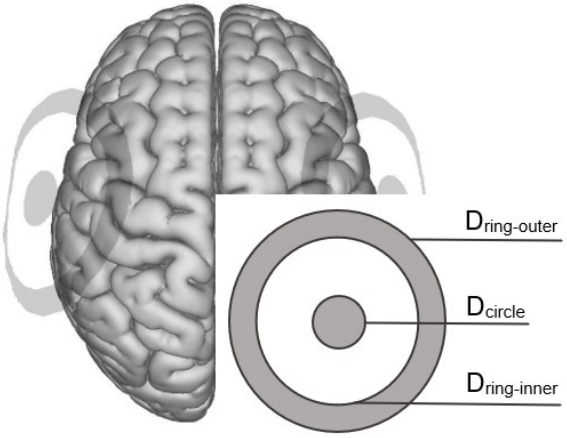

Sizes of the simulated ring electrodes		
D_{circle}	$D_{inner-ring}$	$D_{outer-ring}$
25 mm	78 mm	100 mm
20 mm	30 mm	75 mm
25 mm	30 mm	75 mm
25 mm	90 mm	110 mm
34 mm	70 mm	100 mm
75 mm	90 mm	100 mm
80 mm	90 mm	110 mm

Figure 6 & Table 1: In Figure 6, names of the different diameters of the ring electrodes are specified. In Table 1, the different diameters of electrodes that were simulated are given.

in mm^3. Furthermore, we plotted the direction of the electric field and examined the images of the induced electric field in the SimNIBS GUI.

3.3.1 tACS current values for different phase-lag values

tACS currents are most commonly applied as a sinusoidal wave. Since we assume a quasi-static approximation, we will simulate tACS with a current at a certain point in time. When we have a phase-lag of $\phi = \pi$, the two currents applied to the cortices are in anti-phase. This means that the current values are always opposite: when the current of one cortex is positive, the other cortex will have the same absolute strength but will be negative in value. Thus, for a phase-lag of $\phi = \pi$ we choose the point in time where the current values are at a maximum. The used current values can be found in Table 2.

Table 2: The current values that are used for the tACS simulations of different phase-lag values.

Current values for the different phase-lag value simulations		
	Current value at t1 (A)	*Current value at t2 (A)*
	t1 = 0.0185 s	t2 = 0.13 s
$\phi = 0$	1.09345×10^{-3}	-0.881678×10^{-3}
$\phi = \frac{1}{2}\pi$	-1.02682×10^{-3}	-1.21535×10^{-3}
	t1 = 0.017s	t2 = 0.08s
$\phi = 0$	1.26649×10^{-3}	1.121353×10^{-3}
$\phi = \frac{3}{2}\pi$	0.80374×10^{-3}	-0.881678×10^{-3}
	t1 = 0.0125s	
$\phi = 0$	1.5×10^{-3}	
$\phi = \pi$	-1.5×10^{-3}	

For a phase-lag of $\phi = \frac{1}{2}\pi$ and $\phi = \frac{3}{2}\pi$, the values will not be simply each other's opposites. The point in time that is taken, will influence how the two electric fields in the cortices behave together. This means that the results for the simulations of $\phi = \frac{1}{2}\pi$ and $\phi = \frac{3}{2}\pi$ cannot be generalized to any other point in time. Therefore, for these simulations, we will study an additional point in time. Although we cannot make any generalizations, we can see the similarity of the response of the electric field for two points in time when the phase-lag value is the same. The two points in time that are taken for both phase-lag values can be found in Table 2. The values for the currents were chosen so that at one instance of time the currents in both electrodes were positive/negative, while at the other instance in

time one current is negative and one is positive. Apart from this, the currents were chosen at random from the graphs of the sinusoids, see Figure 7 and 8. In these figures the markers are placed over the instances in time that were chosen for analysis. These values correspond with Table 2.

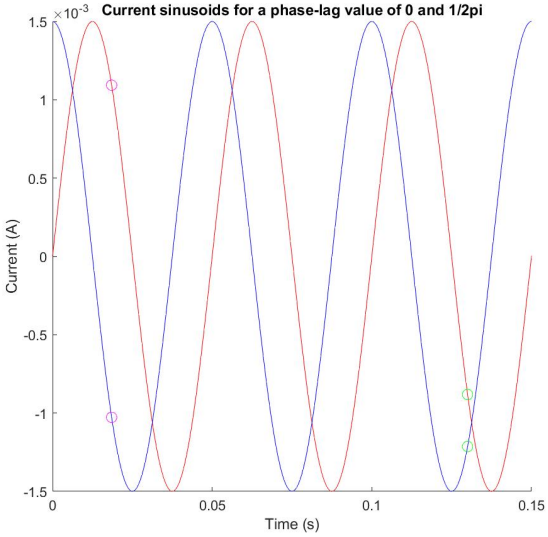

Figure 7: The sinusoidal current functions for the tACS simulations. The red line is the function for a phase-lag of $\phi = 0$, and the blue line is for a phase=lag of $\phi = \frac{1}{2}\pi$. The magenta markers indicate the chosen currents for t1, and the green markers indicate the currents for t2 (see Table 2).

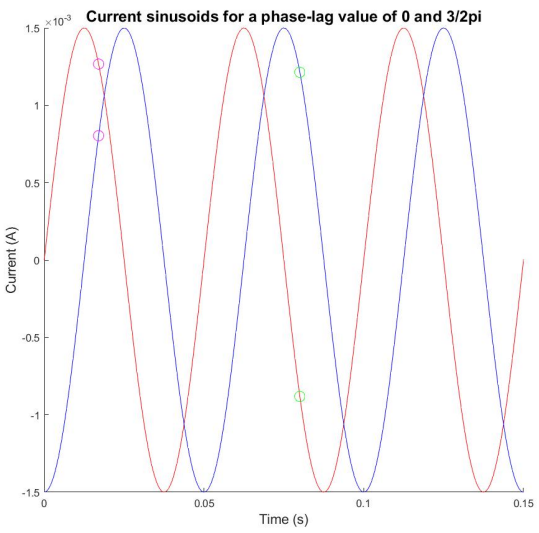

Figure 8: The sinusoidal current functions for the tACS simulations. The red line is the function for a phase-lag of $\phi = 0$, and the blue line is for a phase=lag of $\phi = \frac{3}{2}\pi$. The magenta markers indicate the chosen currents for t1, and the green markers indicate the currents for t2 (see Table 2).

4 Results

In this chapter, the results of the study will be discussed. First, an analysis of the electric fields for different ring electrode montages will be discussed. Then, the 'best' ring electrode montage will be chosen. This montage will be used in the rest of the simulations. Next, the electric fields for the different phase lags between cortices are analyzed. They are first analyzed individually and then compared to each other. Lastly, we will study the direction of the electric field.

4.1 Simulation of different ring electrode montages

The electric fields in the cortices were visualized and analyzed for the different ring electrode montages in Table 1. In Table 3, the maximum field strength in the ROI for both hemispheres is given for the different montages. The highest field strength is achieved with a ring electrode montage of (D_{circle}, $D_{inner-ring}$, $D_{outer-ring}$) = (25, 90, 110). Two other montages that have a relatively high field strength are (25, 78, 100) and (34, 70, 100). In Table 4, the focality in the cortex is given for the different montages. The highest focality is achieved with a ring electrode montage of (D_{circle}, $D_{inner-ring}$, $D_{outer-ring}$) = (25, 30, 75). Three other montages that have a relatively high focality are (20, 30, 75) and, (25, 78, 100), and (34, 70, 100).

Table 3: The maximum peaks of the resulting E-field field strength in the case of different ring electrode montages, for a phase-lag value of $\phi = 0$ and $\phi = \pi$, in the ROI in both hemispheres

Maximum field strength for the ring electrode montages				
	Left hemisphere		Right hemisphere	
Dimensions of electrode (mm)	*Max. strength for $\phi = 0$ (V/m)*	*Max. strength for $\phi = \pi$ (V/m)*	*Max. strength for $\phi = 0$ (V/m)*	*Max. strength for $\phi = \pi$ (V/m)*
20 - 30 - 75	5.59×10^{-2}	5.83×10^{-2}	4.67×10^{-2}	4.14×10^{-2}
25 - 30 - 75	4.87×10^{-2}	5.09×10^{-2}	4.08×10^{-2}	3.47×10^{-2}
25 - 78 - 100	1.21×10^{-1}	1.32×10^{-1}	1.14×10^{-1}	1.19×10^{-1}
25 - 90 - 110	1.37×10^{-1}	1.51×10^{-1}	1.29×10^{-1}	1.37×10^{-1}
34 - 70 - 100	1.04×10^{-1}	1.11×10^{-1}	9.49×10^{-2}	9.90×10^{-2}
75 - 90 - 100	6.12×10^{-2}	7.03×10^{-2}	5.14×10^{-2}	6.40×10^{-2}
80 - 90 - 110	5.29×10^{-2}	6.11×10^{-2}	4.24×10^{-2}	5.51×10^{-2}

Table 4: The focality of the resulting E-field field strength in the case of different ring electrode montages, for a phase-lag value of $\phi = 0$ and $\phi = \pi$

Focality for the ring electrode montages		
Dimensions of electrode (mm)	*Focality in-phase (mm^3)*	*Focality anti-phase (mm^3)*
20 - 30 - 75	5.54×10^3	4.89×10^3
25 - 30 - 75	5.84×10^3	4.99×10^3
25 - 78 - 100	1.17×10^4	1.16×10^4
25 - 90 - 110	1.47×10^4	1.47×10^4
34 - 75 - 100	1.15×10^4	1.15×10^4
75 - 90 - 100	1.69×10^4	1.98×10^4
80 - 90 - 110	1.64×10^4	1.98×10^4

Of the seven ring electrode montages, three montages will be highlighted in this section. The figures and an analysis of the other four montages can be found in Appendix A. The three montages in this

chapter are examples of a compromise between a high electric field strength and a high focality of the electric field.

Simulation - Ring electrode montage (25, 78, 100)

For the simulation with the electrodes where $D_{circle} = 25$ mm, $D_{ring-in} = 78$ mm, and $D_{ring-out} = 100$ mm, the maximum of the electric field strength with the two electrodes in both in-phase and anti-phase is approximately 0.12 V/m (see Figures 9 and 10). For the in-phase simulation, the maximum electric field strength is 1.21×10^{-1} V/m in the left hemisphere and 1.14×10^{-1} V/m in the right hemisphere. For the anti-phase simulation, the maximum electric field strength is 1.32×10^{-1} V/m in the left hemisphere and 1.19×10^{-1} V/m in the right hemisphere. The focality for the in-phase stimulation is 1.17×10^4 mm^3, and 1.16×10^4 mm^3 for the anti-phase stimulation.

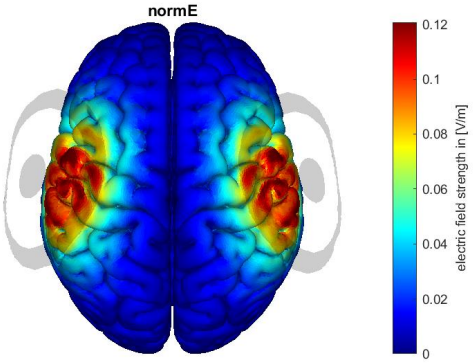

Figure 9: The distribution of the E-field when there is a phase-lag between cortices of 0, with $D_{circular} = 25$ mm, $D_{inner} = 78$ mm, and $D_{outer} = 100$ mm. The maximum electric field strength is approximately 0.12 V/m.

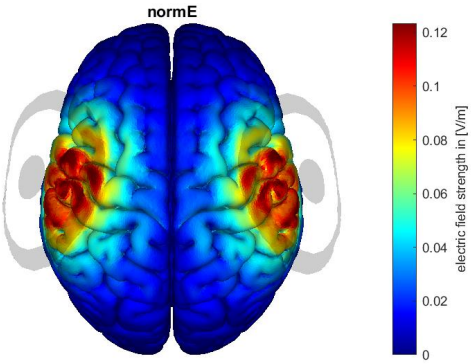

Figure 10: The distribution of the E-field when there is a phase-lag between cortices of π, with $D_{circular} = 25$ mm, $D_{inner} = 78$ mm, and $D_{outer} = 100$ mm. The maximum electric field strength is approximately 0.12 V/m.

Simulation - Ring electrode montage (25, 90, 110)

For the simulation with the electrodes where $D_{circle} = 25$ mm, $D_{ring-in} = 90$ mm, and $D_{ring-out} = 110$ mm, the maximum of the electric field strength with the two electrodes in in-phase and anti-phase are approximately 0.12 V/m and 0.14 V/m, respectively (see Figures 11 and 12). For the in-phase simulation, the maximum electric field strength is 1.37×10^{-1} V/m in the left hemisphere and 1.29×10^{-1} V/m in the right hemisphere. For the anti-phase simulation, the maximum electric field strength is 1.51×10^{-1} V/m in the left hemisphere and 1.37×10^{-1} V/m in the right hemisphere. The focality for the in-phase stimulation is 1.47×10^4 mm^3 and 1.47×10^4 mm^3 for the anti-phase stimulation.

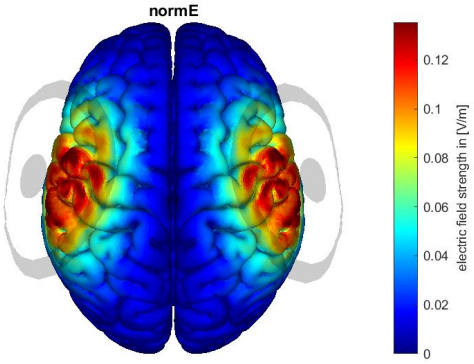

Figure 11: The distribution of the E-field when there is a phase-lag between cortices of 0, with $D_{circular}$ = 25 mm, D_{inner} = 90 mm, and D_{outer} = 110 mm. The maximum electric field strength is approximately 0.14 V/m.

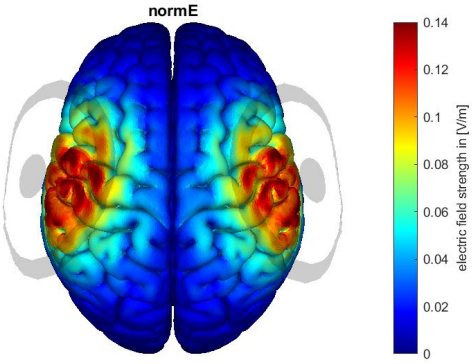

Figure 12: The distribution of the E-field when there is a phase-lag between cortices of π, with $D_{circular}$ = 25 mm, D_{inner} = 90 mm, and D_{outer} = 110 mm. The maximum electric field strength is approximately 0.14 V/m.

Simulation - Ring electrode montage (25, 30, 75)

For the simulation with the electrodes where $D_{circle} = 25$ mm, $D_{ring-in} = 30$ mm, and $D_{ring-out} = 75$ mm, the maximum of the electric field strength with the two electrodes in both in-phase and anti-phase is approximately 0.05 V/m (see Figures 13 and 14). For the in-phase simulation, the maximum electric field strength is 4.87×10^{-2} V/m in the left hemisphere and 4.08×10^{-2} V/m in the right hemisphere. For the anti-phase simulation, the maximum electric field strength is 5.09×10^{-2} V/m in the left hemisphere and 3.47×10^{-2} V/m in the right hemisphere. The focality for the in-phase stimulation is 5.84×10^3 mm^3 and 4.99×10^3 mm^3 for the anti-phase stimulation.

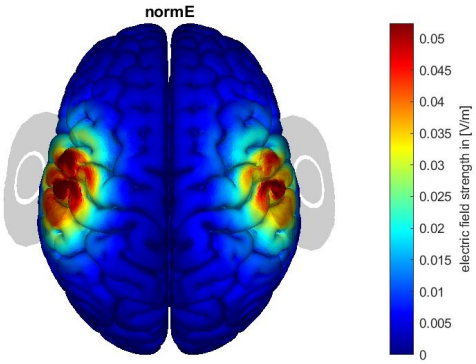

Figure 13: The distribution of the E-field when there is a phase-lag between cortices of 0, with $D_{circular}$ = 25 mm, D_{inner} = 30 mm, and D_{outer} = 75 mm. The maximum electric field strength is approximately 0.055 V/m.

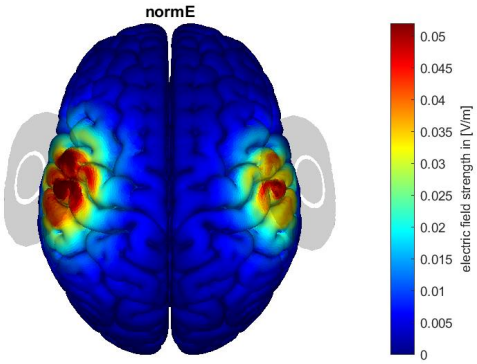

Figure 14: The distribution of the E-field when there is a phase-lag between cortices of π, with $D_{circular}$ = 25 mm, D_{inner} = 30 mm, and D_{outer} = 75 mm. The maximum electric field strength is approximately 0.055 V/m.

4.1.1 Conclusion - Best ring electrode montage

In comparison to the other electrode sizes, the electrode montage with (D_{circle}, $D_{inner-ring}$, $D_{outer-ring}$) = (25, 78, 100) gives a relatively high electric field strength and an intermediate field focality (see Tables 3 and 4). The electrode montage with (D_{circle}, $D_{inner-ring}$, $D_{outer-ring}$) = (25, 90, 110) gives a relatively high electric field strength and a relatively low field focality, while the electrode montage

with (D_{circle}, $D_{inner-ring}$, $D_{outer-ring}$) = (25, 30, 75) gives a relatively low electric field strength and a relatively high field focality.

As mentioned in Chapter 1, it is important to have a compromise between a high strength and a high focality of the electric field. Both the ring electrode montage (25, 78, 100), and (34, 70, 100) have a relatively high field strength and an intermediate field focality (see Tables 3 and 4). Where the electrode montage (25, 78, 100) has a higher field strength, the electrode montage (34, 70, 100) has a (slightly) higher focality. However, the difference in focality is very small when compared to the difference in other montages. The difference in the field strength is relatively big. Thus, out of the different ring electrode montages, the montage (25, 78, 100) seems to be the best configuration. The electric field strength is relatively high, without having a very low focality of the electric field.
This is why, in the simulations of the different phase-lag values between cortices, we will use the ring electrode montage of (D_{circle}, $D_{inner-ring}$, $D_{outer-ring}$) = (25, 78, 100).

4.2 Simulation of different phase-lag values

The electric fields in the cortices were visualized and analyzed for the four different phase-lag values. In Table 5, the average, maximum, and 99.9^{th} percentile of the electric field strength in the ROI in both hemispheres are given. In Table 6, the focality of the electric field for the different phase-lag values is given.

Table 5: The maximum and average strength of the resulting E-field in the ROI in the left and right hemispheres, respectively, for different phase-lag values

Maximum and average electric field strength in the ROI in the right hemisphere			
Phase-lag value	*Average field strength (V/m)*	*Maximum field strength (V/m)*	99.9^{th} *percentile field strength (V/m)*
$\phi = 0$	5.66×10^{-2}	1.193×10^{-1}	1.135×10^{-1}
$\phi = \pi$	6.31×10^{-2}	1.242×10^{-1}	1.188×10^{-1}
$\phi = \frac{1}{2}\pi$	4.59×10^{-2}	9.04×10^{-2}	8.65×10^{-2}
$\phi = \frac{3}{2}\pi$	4.88×10^{-2}	1.015×10^{-1}	9.66×10^{-2}
Maximum and average electric field strength in the ROI in the left hemisphere			
$\phi = 0$	6.08×10^{-2}	1.231×10^{-1}	1.212×10^{-1}
$\phi = \pi$	6.93×10^{-2}	1.334×10^{-1}	1.316×10^{-1}
$\phi = \frac{1}{2}\pi$	4.77×10^{-2}	9.15×10^{-2}	9.03×10^{-2}
$\phi = \frac{3}{2}\pi$	3.13×10^{-2}	6.44×10^{-2}	6.33×10^{-2}

Table 6: The focality of the electric field in the cortices in the simulations of different phase-lag values

Focality of electric field	
Phase-lag value	*Focality*
$\phi = 0$	1.17×10^4
$\phi = \pi$	1.16×10^4
$\phi = \frac{1}{2}\pi$	1.18×10^4
$\phi = \frac{3}{2}\pi$	7.20×10^3

In both hemispheres, the highest average, maximum, and 99.9^{th} percentile of the electric field strength is achieved with a phase-lag of $\phi = \pi$ between the cortices. For the simulations with a phase-lag of $\phi = \frac{1}{2}\pi$ and $\phi = \frac{3}{2}\pi$, the maximum strength of the electric field is relatively low compared to anti-phase simulation (see Table 5). The focality of the electric field is similar for phase-lag values of $\phi = 0$, $\phi = \pi$,

and $\phi = \frac{1}{2}\pi$. The focality for a phase-lag value of $\phi = \frac{3}{2}\pi$ is slightly lower (see Table 6).

When $\phi = 0$, the average field strength is 5.66×10^{-2} V/m in the right hemisphere and 6.08×10^{-2} V/m in the left hemisphere. When $\phi = \pi$, the average field strength is 6.31×10^{-2} V/m in the right hemisphere and 6.93×10^{-2} V/m in the left hemisphere. In both of the simulations, the field strength in the left hemisphere is a bit higher than in the right hemisphere.

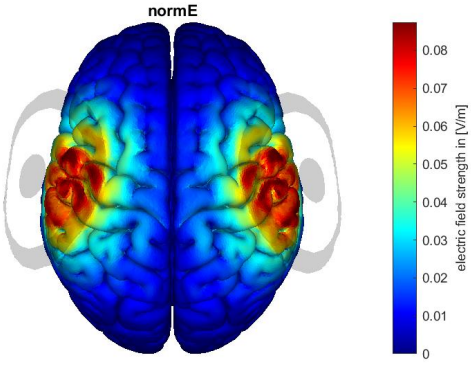

Figure 15: The distribution of the E-field strength when there is a phase-lag between cortices of $\phi = \frac{1}{2}\pi$. The current values for the electrodes are the values at t = 0.0185 s. The maximum electric field strength is approximately 0.085 V/m

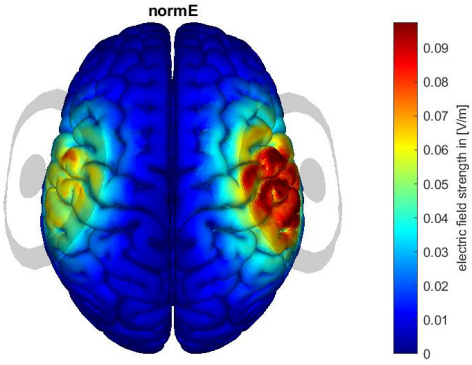

Figure 16: The distribution of the E-field strength when there is a phase-lag between cortices of $\phi = \frac{3}{2}\pi$. The current values for the electrodes are the values at t = 0.0170 s. The maximum electric field strength is approximately 0.095 V/m

For a phase-lag value of $\phi = \frac{1}{2}\pi$, the maximum field strength is approximately 0,085 V/m (see Figure 15). When $\phi = \frac{1}{2}\pi$, the average field strength is 4.59×10^{-2} V/m in the right hemisphere and 4.77×10^{-2} V/m in the left hemisphere (see Table 5). The focality of the electric field is 1.18×10^4 mm^3 (see Table 6). The electric field strength distribution seems similar for the left and the right hemisphere.
For a phase-lag value of $\phi = \frac{3}{2}\pi$, the maximum field strength is approximately 0,095 V/m (see Figure 16). When $\phi = \frac{3}{2}\pi$, the average field strength is 4.88×10^{-2} V/m in the right hemisphere and 3.13×10^{-2} V/m in the left hemisphere (see Table 5). The focality of the electric field is 7.20×10^3 mm^3 (see Table 6). The electric field strength in the right hemisphere is higher than in the left hemisphere. The focality of stimulation seems a little higher in the left hemisphere than in the right hemisphere.

4.2.1 Difference in electric field strength between simulations

In Figures 17, 18, and 19, the electric field distribution in the simulations of $\phi = \pi$, $\phi = \frac{1}{2}\pi$, and $\phi = \frac{3}{2}\pi$, respectively, are compared to the electric field distribution of the in-phase simulation. The figures show the difference in electric field strength between two different phase-lag simulations. The difference in electric field strength is the lowest for $\phi = \pi$. The maximum difference in electric fields is approximately 0.0155 V/m. The difference in the electric field strength seems to be centered around the great longitudinal fissure, in between the two ring electrode montages (see Figure 17). The difference in electric field strength is approximately 13% of the total electric field strength for $\phi = 0$.
The maximum difference in electric field strength between the phase-lags $\phi = 0$ and $\phi = \frac{1}{2}$ is approximately 0.035 V/m. The difference in electric field strength seems to be located mostly at the location of the ring electrode montages.

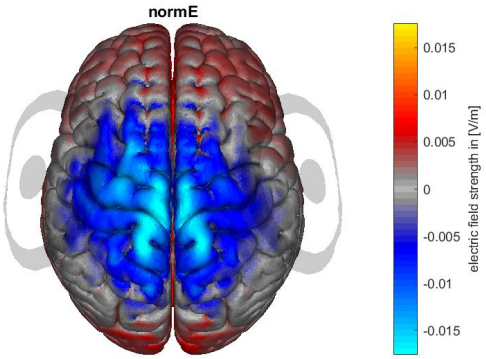

Figure 17: The difference in electric field strength between the simulation for $\phi = 0$ and $\phi = \pi$. The maximum of the electric field difference is approximately 0.0155 V/m.

There is also a difference of approximately 0.01 V/m located around the great longitudinal fissure, in between the two ring electrode montages (see Figure 18). When comparing Figure 9 and 15, we can see that there is indeed a difference in the maximum electric field strength at the location of the ring electrode montage. In Table 5, we can see that this difference is $1.231 \times 10^{-1} - 0.915 \times 10^{-1} = 0.316 \times 10^{-1}$ V/m, which matches Figure 18. The maximum difference is located in the left hemisphere. This difference in electric field strength is approximately 26% of the maximum field strength in the left hemisphere for $\phi = 0$.

The maximum difference in electric field strength between the phase-lags $\phi = 0$ and $\phi = \frac{3}{2}$ is approximately 0.05 V/m. The difference in electric field strength seems to be located mostly at the location of the ring electrode montages. The difference seems stronger in the left hemisphere than in the right hemisphere (see Figure 19). When comparing Figure 9 and 16, we can see that there is indeed a difference in the maximum electric field strength at the location of the ring electrode montage. It is also visible that the electric field strength is lower in the left hemisphere, logically creating a bigger difference when compared to the in-phase stimulation. In Table 5, we can see that this difference is 1.231×10^{-1} V/m $- 0.644 \times 10^{-1}$ V/m $= 0.587 \times 10^{-1}$ V/m, which matches Figure 19. This difference in electric field strength is approximately 48% of the maximum field strength in the left hemisphere for $\phi = 0$.

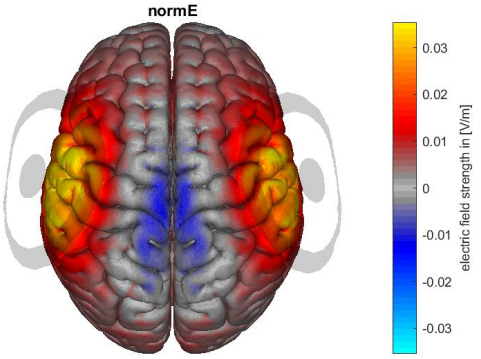

Figure 18: The difference in electric field strength between the simulation for $\phi = 0$ and $\phi = \frac{1}{2}\pi$. The current values for the electrodes with a phase-lag of $\phi = \frac{1}{2}\pi$ are the values at t = 0.0185 s. The maximum of the electric field difference is approximately 0.035 V/m.

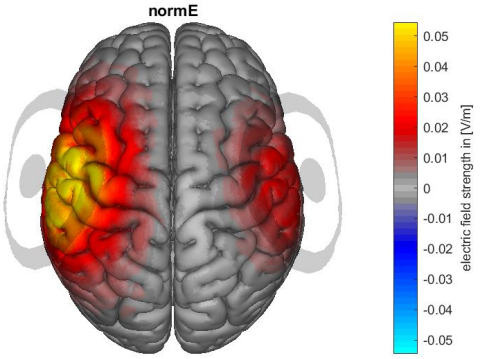

Figure 19: The difference in electric field strength between the simulation for $\phi = 0$ and $\phi = \frac{3}{2}\pi$. The current values for the electrodes with a phase-lag of $\phi = \frac{3}{2}\pi$ are the values at t = 0.0170 s. The maximum of the electric field difference is approximately 0.05 V/m.

4.2.2 The direction of the electric field for the phase-lag values

In Figure 20, the direction of the electric field in the cortex is visualized. For the phase-lag value of $\phi = 0$, the direction of the electric field seems perpendicular to the cortex for high electric field strengths. When the electric field strength gets weaker, the direction of the electric field becomes more parallel to the cortex.

When studying the direction of the electric field, one peak in the electric field seems to be located outside of the main focality of the field. Figure 20 shows an enlarged picture of the electrode above the right hemisphere. The red circle indicates the position of the peak that seems to be an outlier. There do not seem to be any more of these peaks in either the right or the left hemisphere.

The direction of the electric field was plotted for all phase-lag values. The figures for a phase-lag of $\phi = \pi$, $\phi = \frac{1}{2}\pi$, and $\phi = \frac{3}{2}\pi$ can be found in Appendix C. In all these figures, the electric field seems to behave as expected. The peak located outside of the main focality of the electric field seems to be present in the simulations of all phase-lag values.

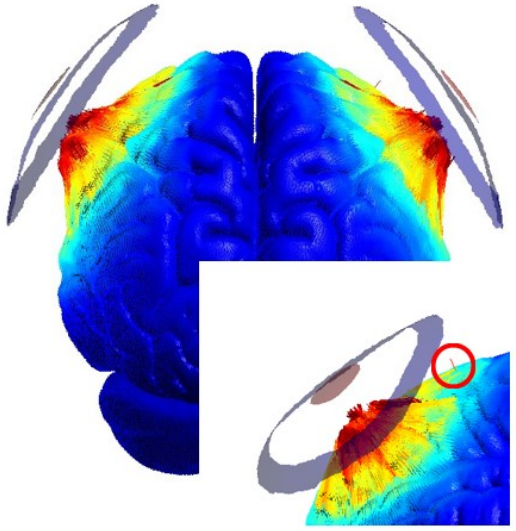

Figure 20: A figure of the simulation where the direction of the electric field is visible. The phase-lag value for the simulation is $\phi = 0$. The electric field is perpendicular to the cortex in areas where the electric field strength is high (see the dark-red areas in the figure). The electric field gradually changes to be more parallel to the cortex in areas where the electric field strength is lower (see the green/blue areas). The red circle in the figure indicates the position of a field peak in the right hemisphere that seems to lie out of the main focality of the field.

4.2.3 Additional points in time for phase-lag values

The simulations for phase-lag values of $\phi = \frac{1}{2}\pi$ and $\phi = \frac{3}{2}\pi$ were also done for different current values, see Chapter 3). In Tables 7 and 8, the average, maximum, and 99.9^{th} percentile of the electric field strength is compared for the two instances in time. For the phase-lag of $\phi = \frac{1}{2}\pi$, the currents for simulation were taken at $t_1 = 0.0185$ s and $t_2 = 0.13$ s. For the phase-lag of $\phi = \frac{3}{2}\pi$ these time instances were $t_1 = 0.017$ s and $t_2 = 0.08$ s. In Figures 21 and 22, the electric field distribution in the two additional time instances can be seen.

Table 7: The maximum and average strength of the resulting E-field in the ROI in the left and right hemispheres, respectively, for different time instances for a phase-lag value of $\phi = \frac{1}{2}\pi$.

Maximum and average electric field strength in the ROI for a phase-lag value of $\phi = \frac{1}{2}\pi$.				
Hemisphere	*Time (s)*	*Average E-field (V/m)*	*Max. E-field (V/m)*	99.9^{th} *p. E-field (V/m)*
left	0.0185	0.0459	0.0904	0.0865
right	0.0185	0.0477	0.0915	0.0903
left	0.13	0.0326	0.0696	0.0661
right	0.13	0.0501	0.1008	0.0992

Simulation of the phase-lag $\phi = \frac{1}{2}\pi$ with a different current

For the simulation with a phase-lag value of $\phi = \frac{1}{2}\pi$, at t = 0.13 s, the maximum electric field strength is approximately 0.095 V/m (see Figure 21). The average electric field strength is 3.26×10^{-2} V/m in the left hemisphere and 5.01×10^{-2} V/m in the right hemisphere. The focality of the electric field is 7.38×10^3 mm^3. The average, maximum, and 99.9^{th} percentile of the electric field for t = 0.0185 s and t = 0.13 s are not the same.

When comparing the figures for $\phi = \frac{1}{2}\pi$ at t = 0.0185 s (Figure 15) and t = 0.13 s (Figure 21), we see that the maximum of the electric field strength in the right hemisphere is a bit higher for the current at t = 0.13 s. The maximum electric field strength in the left hemisphere is a bit lower for the current at t = 0.13 s. While at t = 0.0185 s the electric field distribution is similar for both hemispheres, we see a difference for t = 0.13 s. The electric field strength in the right hemisphere is lower than in the right hemisphere.

Table 8: The maximum and average strength of the resulting E-field in the ROI in the left and right hemispheres, respectively, for different phase-lag values. for different time instances for a phase-lag value of $\phi = \frac{3}{2}\pi$.

Maximum and average electric field strength in the ROI for a phase-lag value of $\phi = \frac{3}{2}\pi$.				
Hemisphere	*Time (s)*	*Average E-field (V/m)*	*Max. E-field (V/m)*	99.9^{th} *p. E-field (V/m)*
left	0.017	0.0488	0.1050	0.0966
right	0.017	0.0313	0.0644	0.0633
left	0.08	0.0528	0.1091	0.1040
right	0.08	0.0239	0.0500	0.0491

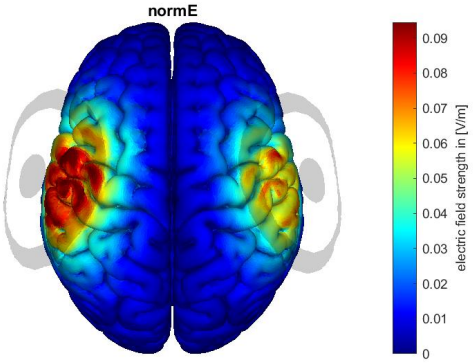

Figure 21: The distribution of the E-field strength when there is a phase-lag value of $\phi = \frac{1}{2}\pi$. The current values for the electrodes are the values at t = 0.13 s. The maximum electric field strength is approximately 0.095 V/m

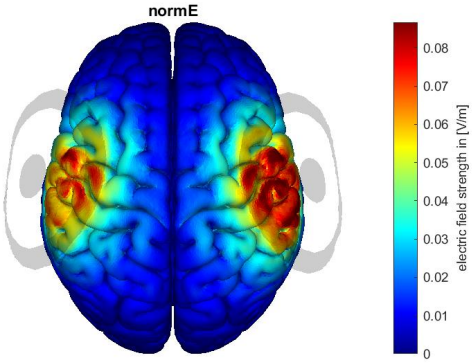

Figure 22: The distribution of the E-field strength when there is a phase-lag value of $\phi = \frac{3}{2}\pi$. The current values for the electrodes are the values at t = 0.08s. The maximum electric field strength is approximately 0.085 V/m

Simulation of the phase-lag $\phi = \frac{3}{2}\pi$ with a different current
For the simulation with a phase-lag value of $\phi = \frac{3}{2}\pi$, at t = 0.08 s, the maximum electric field strength is approximately 0.085 V/m (see Figure 22). The average electric field strength is 5.28×10^{-2} V/m in the left hemisphere and 2.39×10^{-2} V/m in the right hemisphere. The focality of the electric field is 9.32×10^{3} mm^3. The average, maximum, and 99.9^{th} percentile of the electric field for t = 0.017 s and t = 0.08 s are also not the same.

When comparing the figures for $\phi = \frac{3}{2}\pi$ at t = 0.017 s (Figure 16) and t = 0.08 s (Figure 22), we see that the maximum of the electric field strength in the right hemisphere is a bit higher for the current at t = 0.017 s. The maximum electric field strength in the left hemisphere is a bit higher for the current at t = 0.08 s. While at t = 0.0185 s the electric field distribution is similar for both hemispheres, we see a difference for t = 0.13 s. The electric field strength in the right hemisphere is lower than in the right hemisphere.

For the simulations with $\phi = \frac{1}{2}\pi$ and $\phi = \frac{3}{2}\pi$, different currents are applied between simulations at different instances of time (see Chapter 3.1.1). The relation between the maximum strength of the electric field and the applied tACS currents was investigated. In Figures (..), the two parameters are plotted against each other. It is visible, that the maximum strength of the electric field increases when the applied tACS current increases. This seems to be true for both hemispheres. However, when we compare in which hemisphere the peak of the electric field strength is located, to in which hemisphere we have applied the highest current, we find a contradictory result. For $\phi = \frac{1}{2}\pi$ at t = 0.13 s and $\phi = \frac{3}{2}\pi$ at both time instances, the maximum electric field strength is located in the same hemisphere as the highest applied current. However, for $\phi = \frac{1}{2}\pi$ at t = 0.0185 s, this is not the case, see Table 9. In this table, we can see that the difference in tACS currents between both hemispheres is approximately a factor 3.6 smaller than the smallest difference in currents for the other simulations.

Table 9: Comparison of the hemisphere with the highest applied tACS currents and the hemisphere where the maximum field strength is located

Locations of the highest tACS current and hemisphere with the maximum E-field strength			
Phase-lag value	*tACS current (A)*	*Hemisphere with E-field$_{max}$*	*Abs(ΔC) (A)*
$\phi = \frac{1}{2}\pi$	1.09345×10^{-3}	Left	0.06663×10^{-3}
$\phi = \frac{1}{2}\pi$	-1.211353×10^{-3}	Right	0.46275×10^{-3}
$\phi = \frac{3}{2}\pi$	1.26649×10^{-3}	Left	0.239683×10^{-3}
$\phi = \frac{3}{2}\pi$	1.121353×10^{-3}	Right	0.239683×10^{-3}

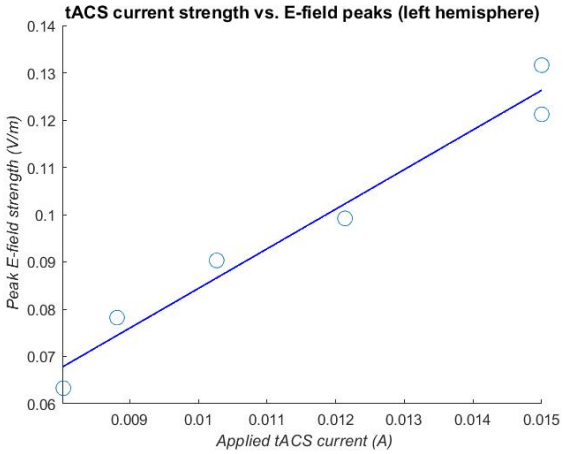

Figure 23: The values for the applied (absolute) tACS currents in the left hemisphere (x-axis) plotted against the peak E-field strength (y-axis). The blue circles indicate the different applied currents. The blue line is a plotted polynomial of degree 1. The maximum E-field strength increases as the applied current increases.

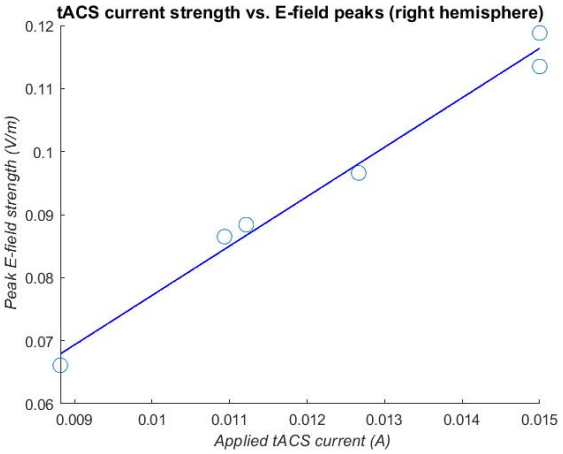

Figure 24: The values for the applied (absolute) tACS currents in the right hemisphere (x-axis) plotted against the peak E-field strength (y-axis). The blue circles indicate the different applied currents. The blue line is a plotted polynomial of degree 1. The maximum E-field strength increases as the applied current increases.

Comparison to the in-phase simulation and analysis of direction of field

The simulations with $\phi = \frac{1}{2}\pi$ and $\phi = \frac{3}{2}\pi$ were also compared to the in-phase simulation. Figure 34 and 35 (see Appendix B) show the difference in electric field strength between the in-phase simulation and the $\phi = \frac{1}{2}\pi$ and $\phi = \frac{3}{2}\pi$ simulations, respectively.

The maximum difference in electric field strength between the phase-lags $\phi = 0$ and $\phi = \frac{1}{2}$ at t = 0.13 s is approximately 0.045 V/m. The difference in electric field strength seems to be located mostly below location of the ring electrode montages. The difference seems stronger in the right hemisphere than in the left hemisphere (see Figure 34). The current applied to the right hemisphere was -0.88167×10^{-3} A, while the current applied to the left hemisphere was -1.21353×10^{-3} A. When comparing the figures with the electric field distribution for $\phi = 0$ and $\phi = \frac{1}{2}\pi$ (Figure 9 and 21), we can see that there is indeed a difference in the maximum electric field strength below the ring electrode montage. It is also visible that the electric field strength is lower in the right hemisphere, logically creating a bigger difference when compared to the in-phase stimulation. In Tables 5 and 7, we can see that the difference in maximum field strength is given by 1.193×10^{-1} V/m $- 0.696 \times 10^{-1}$ V/m $= 0.535 \times 10^{-1}$ V/m, which matches Figure 34. This difference is approximately 58% of the peak strength in the right hemisphere for $\phi = 0$.

The maximum difference in electric field strength between the phase-lags $\phi = 0$ and $\phi = \frac{3}{2}$ at t = 0.08 s is approximately 0.045 V/m. Also here, the difference in electric field strength is located below the ring electrodes. The difference seems stronger in the left hemisphere than in the right hemisphere (see Figure 35). The current applied to the left hemisphere was 1.21353×10^{-3} A, while the current applied

to the left hemisphere was -0.881678×10^{-3} A. When we compare the electric field distribution of $\phi = 0$ to the one of $\phi = \frac{3}{2}\pi$ (Figure 9 and 22), we see that the location of the difference in electric field is below the ring electrode. There is a difference of approximately 0.01 V/m located around the great longitudinal fissure, in between the two ring electrode montages. In Tables 5 and 7, we can see that this difference is 1.231×10^{-1} V/m $- 0.500 \times 10^{-1}$ V/m $= 0.731 \times 10^{-1}$ V/m, which matches Figure 35. This difference is approximately 60% of the peak strength in the left hemisphere.

For the simulations with the phase-lag values of $\phi = \frac{1}{2}\pi$ and $\phi = \frac{3}{2}\pi$, we also plotted the direction of the electric field. Figure 39 and 40 show the direction of the electric field for $\phi = \frac{1}{2}\pi$, t = 0.13 s and $\phi = \frac{3}{2}\pi$, t = 0.08 s, respectively. The figures can be found in Appendix C. The electric field behaves as expected in both simulations. Also in these simulations, the peak located outside of the main focality in the right hemisphere is present.

5 Conclusion

In this study, we have analyzed the changes in the dual-site tACS-induced electric fields, as a result of changing the size of stimulation ring electrodes and the phase-lag values between the primary motor cortices. As a result of changing the size of stimulation ring electrodes, the induced electric fields differed in the focality and strength of the electric field. A compromise for a high focality and high strength of the electric field was found in the ring electrode montage where (D_{circle}, $D_{inner-ring}$, $D_{outer-ring}$) = (25, 78, 100). The maximum electric field strength for a simulation with for a phase-lag of $\phi = 0$ in the left hemisphere is 1.21×10^{-1} V/m, and 1.14×10^{-1}V/m for the right hemisphere. For a phase-lag of $\phi = \pi$ the maximum field strength is 1.32×10^{-1} in the left hemisphere and 1.19×10^{-1} in the right hemisphere. The focality of the electric field is $1.17 \times 10^{3} mm^{3}$ for $\phi = 0$ and $1.16 \times 10^{3} mm^{3}$ for $\phi = \pi$. Of the different ring electrode montages that were tested, this montage seems to give us the best compromise between the focality and strength of the electric field.

The focality and strength of the electric field are also influenced by changing the phase-lag values between cortices. When a phase-lag of $\phi = \frac{1}{2}\pi$ or $\phi = \frac{3}{2}\pi$ is applied, the maximum field strength and focality are a little lower than for the in- and anti-phase stimulation. For the phase-lag values of $\phi = \frac{1}{2}\pi$ and $\phi = \frac{3}{2}\pi$, applied tACS currents for two instances in time were analyzed. In these simulations, there was a distinct difference in field strength and focality between the two hemispheres. This difference is likely due to the difference in the applied tACS current. In both hemispheres, the maximum electric field strength is higher when the applied tACS current increases. However, at $\phi = \frac{1}{2}\pi$ at t = 0.0185 s the maximum of the electric field is located in the left hemisphere, while the highest tACS current is applied to the right hemisphere. This is contradictory to the other results. However, the difference in the applied tACS currents between the hemispheres is smaller than for the other simulations. This decrease in difference and the fluctuations between hemispheres due to anatomical differences could be responsible for this unexpected result.

By comparing the simulations of the different time instances and difference phase-lag values, we can see that when the currents are chosen to be both negative or both positive, there is no difference in stimulation at the great longitudinal fissure. However, when one of the currents is negative and one is positive, this difference seems to be present. In the stimulations with $\phi = \frac{1}{2}\pi$ at t = 0.13 s and $\phi = \frac{3}{2}\pi$ at t = 0.08 s, the same absolute tACS current values are used. However, for $\phi = \frac{1}{2}\pi$ both currents have a negative value, while for $\phi = \frac{3}{2}\pi$ one current has a positive value, and the other current a negative value. The peaks of the E-field are similar for the two simulations, while the difference in electric field strength (compared to $\phi = 0$) at the great longitudinal fissure is only present for $\phi = \frac{3}{2}\pi$ at t = 0.08 s. This could be comparable to the anti-phase stimulation, where one current is positive and one negative and the difference around the great longitudinal fissure is also present.

The direction of the electric field gradually changed from perpendicular to the cortex to a more parallel orientation to the cortex for all phase-lag simulations. A peak outside of the ROI was found for all phase-lag simulations, at approximately the same position. However, the volume of this peak is considered insignificant compared to the volume of the main peak of the electric field.

In this study, we have found more information on how the electric field induced by tACS responds to different settings of stimulation. We have analyzed the different ring electrode montages to find an optimized compromise within the scope of this experiment. Furthermore, we have studied how the electric field changes when we apply different phase lags between cortices. With all this data, we understand the behavior of the electric field a little better. For example, we have seen a change in the maximum electric field strength as a result of changing the phase lags in our simulation. Thus, we now know a bit more about how we can influence electric fields induced by tACS. We also have a better idea of what research needs to be done to increase this understanding and expand on this research protocol.

6 Discussion

In this study, we gained more insight into the settings of stimulation that can influence the electric field induced by tACS. While we gained new insights, the results are limited by their generalizability. With more research, the generalizability of the results could be expanded and new insights could be made. Here, we will discuss the implications and limitations of our research and discuss possibilities for further research.

Firstly, this study could be expanded by studying the relation between the resulting electric field characteristics in additional ways. Due to the time constraints for this study, a choice for studying certain characteristics was made. Using the data from SimNIBS and Matlab used in this paper, some characteristics could be studied in more detail. For example, the direction of the induced electric field as a comparison between different phase-lag values could be studied.

For the phase-lag values of $\phi = \frac{1}{2}\pi$ and $\phi = \frac{3}{2}\pi$, we studied two instances of time. In Chapter 3.3.1, we explained that studying one point in time for these phase-lag values would lead to results that cannot be generalized. The tACS current is applied as a sinusoidal wave, meaning that after every period, the current wave repeats. However, within the period there is no repetition as there is only a single wave. Thus, when we choose an arbitrary point in time t_1 and an arbitrary point in time t_2, they will have a different current value. Therefore, within the period of the wave, we cannot generalize over points of time. Our results are therefore only valid for the chosen phase-lag at the exact points of time that we have chosen. While we have studied induced electric field when we choose a point in time where both currents are positive or negative, or one is positive and one negative, we cannot accurately predict the electric field in different instances of time. Further research is needed to study more instances of time and see if the results could be generalized.

In the simulations, the ROI was located by choosing the MNI coordinates for M1 based on the activation likelihood estimation (ALE) of M1[42]. The ROI is approximated by taking the MNI coordinate as the center of our ROI and having a sphere with a diameter of 10 mm around the center of the ROI to define its boundaries. However, the shape of the ROI as defined in our study does not cover the full area of M1. In Figure 25, we can see that the primary motor cortex covers a more long-stretched area. While our results do tell us about the strength within part of M1, the results cannot be generalized to the entire M1. Future research could include a more accurate representation of the area of M1 for analysis. This could, for example, be done by defining the ROI in an atlas.

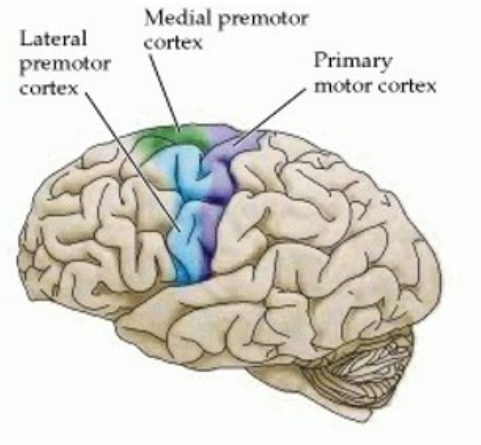

Figure 25: In the figure the primary motor cortex is indicated in purple. M1 covers a narrow, and long area in the frontal lobe of the brain. Figure from [43].

For all simulations, there is a difference in electric field strength and focality between the left and right hemispheres. This difference could be explained by the asymmetry of the human brain[39]. All human brains have an asymmetry to a certain degree, and the head model used in the simulation is expected to reflect these differences. Templates with symmetric head models are available, however, we believe it to be useful to simulate with an asymmetric head model. While brain anatomy varies per subject, generally, functional brain asymmetry has been observed [44]. Thus, the asymmetry in the model presents us with more realistic data, than a symmetrical model would. However, more research on how this asymmetry influences the difference in the electric fields of both hemispheres during tACS should be done.

Individual brain anatomy might be the cause of variability in the strength and focality of the electric field induced by tES [45]. With our current model, we cannot study the exact influence of changing settings of stimulation on the tACS-induced electric field. However, if more knowledge of the physiological mechanisms behind tACS is gained, we could use models like these to accurately predict the results of tACS. To account for individual brain anatomy, MRI scans of a patient can be used to create a personalized head model for tACS preparation. While the individualizing of tACS modeling might be quite time-consuming and costly, with an eye on the future it could be beneficial to do further research on this.

References

[1] T. Reed and R. Cohen Kadosh, "Transcranial electrical stimulation (tES) mechanisms and its effects on cortical excitability and connectivity," *Journal of Inherited Metabolic Disease*, vol. 41, no. 6, p. 1123, Nov. 2018, ISSN: 15732665. DOI: 10.1007/S10545-018-0181-4. [Online]. Available: /pmc/articles/PMC6326965/%20/pmc/articles/PMC6326965/?report=abstract%20https://www.ncbi.nlm.nih.gov/pmc/articles/PMC6326965/.

[2] A. V. Tavakoli and K. Yun, "Transcranial alternating current stimulation (tACS) mechanisms and protocols," *Frontiers in Cellular Neuroscience*, vol. 11, p. 214, Sep. 2017, ISSN: 16625102. DOI: 10.3389/FNCEL.2017.00214/BIBTEX.

[3] A. Antal and W. Paulus, "Transcranial alternating current stimulation (tACS)," *Frontiers in Human Neuroscience*, no. JUN, Jun. 2013, ISSN: 16625161. DOI: 10.3389/fnhum.2013.00317.

[4] O. Elyamany, G. Leicht, C. S. Herrmann, and C. Mulert, "Transcranial alternating current stimulation (tACS): from basic mechanisms towards first applications in psychiatry," *European Archives of Psychiatry and Clinical Neuroscience 2020 271:1*, vol. 271, no. 1, pp. 135–156, Nov. 2020, ISSN: 1433-8491. DOI: 10.1007/S00406-020-01209-9. [Online]. Available: https://link.springer.com/article/10.1007/s00406-020-01209-9.

[5] R. C. Cole, D. N. Okine, B. E. Yeager, and N. S. Narayanan, "Neuromodulation of cognition in Parkinson's disease," *Progress in brain research*, vol. 269, no. 1, p. 435, Jan. 2022, ISSN: 18757855. DOI: 10.1016/BS.PBR.2022.01.016. [Online]. Available: /pmc/articles/PMC9199111/%20/pmc/articles/PMC9199111/?report=abstract%20https://www.ncbi.nlm.nih.gov/pmc/articles/PMC9199111/.

[6] S. Ahn *et al.*, "Targeting reduced neural oscillations in patients with schizophrenia by transcranial alternating current stimulation," *NeuroImage*, vol. 186, pp. 126–136, Feb. 2019, ISSN: 1053-8119. DOI: 10.1016/J.NEUROIMAGE.2018.10.056. [Online]. Available: https://linkinghub.elsevier.com/retrieve/pii/S1053811918320287.

[7] M. Fiene, B. C. Schwab, J. Misselhorn, C. S. Herrmann, T. R. Schneider, and A. K. Engel, "Phase-specific manipulation of rhythmic brain activity by transcranial alternating current stimulation," *Brain Stimulation*, vol. 13, no. 5, pp. 1254–1262, Sep. 2020, ISSN: 1935-861X. DOI: 10.1016/J.BRS.2020.06.008.

[8] A. Berger, N. H. Pixa, F. Steinberg, and M. Doppelmayr, "Brain oscillatory and hemodynamic activity in a bimanual coordination task following transcranial alternating current stimulation (TACS): A combined EEG-fNIRS study," *Frontiers in Behavioral Neuroscience*, vol. 12, Apr. 2018, ISSN: 16625153. DOI: 10.3389/FNBEH.2018.00067/FULL. [Online]. Available: /pmc/articles/PMC5915568/%20/pmc/articles/PMC5915568/?report=abstract%20https://www.ncbi.nlm.nih.gov/pmc/articles/PMC5915568/.

[9] L. Wu, T. Liu, and J. Wang, "Improving the Effect of Transcranial Alternating Current Stimulation (tACS): A Systematic Review," *Frontiers in Human Neuroscience*, vol. 15, p. 255, Jun. 2021, ISSN: 16625161. DOI: 10.3389/FNHUM.2021.652393/XML/NLM.

[10] T. O. Bergmann and G. Hartwigsen, "Inferring Causality from Noninvasive Brain Stimulation in Cognitive Neuroscience," 2020. DOI: 10.1162/jocn{_}a{_}01591. [Online]. Available: https://doi.org/10.1162/jocn_a_01591.

[11] L. Haberbosch *et al.*, "Rebound or entrainment? The influence of alternating current stimulation on individual alpha," *Frontiers in Human Neuroscience*, vol. 13, p. 43, Feb. 2019, ISSN: 16625161. DOI: 10.3389/FNHUM.2019.00043/BIBTEX.

[12] M. Orendáčová and E. Kvašňák, "Effects of Transcranial Alternating Current Stimulation and Neurofeedback on Alpha (EEG) Dynamics: A Review," *Frontiers in Human Neuroscience*, vol. 15, p. 358, Jul. 2021, ISSN: 16625161. DOI: 10.3389/FNHUM.2021.628229/BIBTEX.

[13] K. A. Williams, Y. Cabral-Calderin, C. Schmidt-Samoa, C. A. Weinrich, P. Dechent, and M. Wilke, "Simultaneous Transcranial Alternating Current Stimulation and Functional Magnetic Resonance Imaging," *Journal of Visualized Experiments : JoVE*, vol. 2017, no. 124, p. 55 866, Jun. 2017, ISSN: 1940087X. DOI: 10.3791/55866. [Online]. Available: /pmc/articles/PMC5527955/%20/pmc/articles/PMC5527955/?report=abstract%20https://www.ncbi.nlm.nih.gov/pmc/articles/PMC5527955/.

[14] B. C. Schwab, P. König, and A. K. Engel, "Spike-timing-dependent plasticity can account for connectivity aftereffects of dual-site transcranial alternating current stimulation," *NeuroImage*, vol. 237, Aug. 2021, ISSN: 10959572. DOI: 10.1016/j.neuroimage.2021.118179.

[15] S. Kohli and A. J. Casson, "Removal of Gross Artifacts of Transcranial Alternating Current Stimulation in Simultaneous EEG Monitoring," *Sensors (Basel, Switzerland)*, vol. 19, no. 1, Jan. 2019, ISSN: 1424-8220. DOI: 10.3390/S19010190. [Online]. Available: https://pubmed.ncbi.nlm.nih.gov/30621077/.

[16] K. Wendel *et al.*, "EEG/MEG source imaging: Methods, challenges, and open issues," *Computational Intelligence and Neuroscience*, vol. 2009, 2009, ISSN: 16875265. DOI: 10.1155/2009/656092.

[17] S. P. Singh, "Magnetoencephalography: Basic principles," *Annals of Indian Academy of Neurology*, vol. 17, no. Suppl 1, S107, 2014, ISSN: 19983549. DOI: 10.4103/0972-2327.128676. [Online]. Available: /pmc/articles/PMC4001219/%20/pmc/articles/PMC4001219/?report=abstract%20https://www.ncbi.nlm.nih.gov/pmc/articles/PMC4001219/.

[18] S. Vogeti, C. Boetzel, and C. S. Herrmann, "Entrainment and Spike-Timing Dependent Plasticity – A Review of Proposed Mechanisms of Transcranial Alternating Current Stimulation," *Frontiers in Systems Neuroscience*, vol. 16, p. 19, Feb. 2022, ISSN: 16625137. DOI: 10.3389/FNSYS.2022.827353/BIBTEX.

[19] D. Strüber, S. Rach, T. Neuling, and C. S. Herrmann, "On the possible role of stimulation duration for after-effects of transcranial alternating current stimulation," *Frontiers in Cellular Neuroscience*, vol. 9, no. AUGUST, Aug. 2015, ISSN: 16625102. DOI: 10.3389/fncel.2015.00311.

[20] T. Zaehle, S. Rach, and C. S. Herrmann, "Transcranial Alternating Current Stimulation Enhances Individual Alpha Activity in Human EEG," *PLOS ONE*, vol. 5, no. 11, e13766, 2010, ISSN: 1932-6203. DOI: 10.1371/JOURNAL.PONE.0013766. [Online]. Available: https://journals.plos.org/plosone/article?id=10.1371/journal.pone.0013766.

[21] F. Fröhlich, "Endogenous and exogenous electric fields as modifiers of brain activity: rational design of noninvasive brain stimulation with transcranial alternating current stimulation," *Dialogues in Clinical Neuroscience*, vol. 16, no. 1, p. 93, 2014, ISSN: 12948322. DOI: 10.31887/DCNS.2014.16.1/FFROEHLICH. [Online]. Available: /pmc/articles/PMC3984895/%20/pmc/articles/PMC3984895/?report=abstract%20https://www.ncbi.nlm.nih.gov/pmc/articles/PMC3984895/.

[22] B. C. Preisig and A. Hervais-Adelman, "The Predictive Value of Individual Electric Field Modeling for Transcranial Alternating Current Stimulation Induced Brain Modulation," *Frontiers in Cellular Neuroscience*, vol. 16, p. 67, Feb. 2022, ISSN: 16625102. DOI: 10.3389/FNCEL.2022.818703/BIBTEX.

[23] K. F. Heise *et al.*, "Evaluation of a Modified High-Definition Electrode Montage for Transcranial Alternating Current Stimulation (tACS) of Pre-Central Areas," *Brain Stimulation*, vol. 9, no. 5, pp. 700–704, Sep. 2016, ISSN: 1935-861X. DOI: 10.1016/J.BRS.2016.04.009.

[24] A. Datta, M. Elwassif, F. Battaglia, and M. Bikson, "Transcranial current stimulation focality using disc and ring electrode configurations: FEM analysis," *Journal of Neural Engineering*, vol. 5, no. 2, p. 163, Apr. 2008, ISSN: 1741-2552. DOI: 10.1088/1741-2560/5/2/007. [Online]. Available: https://iopscience.iop.org/article/10.1088/1741-2560/5/2/007%20https://iopscience.iop.org/article/10.1088/1741-2560/5/2/007/meta.

[25] I. Alekseichuk *et al.*, "Electric field dynamics in the brain during multi-electrode transcranial electric stimulation," *Nature communications*, vol. 10, no. 1, Dec. 2019, ISSN: 2041-1723. DOI: 10.1038/S41467-019-10581-7. [Online]. Available: https://pubmed.ncbi.nlm.nih.gov/31189931/.

[26] B. C. Schwab, J. Misselhorn, and A. K. Engel, "Modulation of large-scale cortical coupling by transcranial alternating current stimulation," *Brain Stimulation*, vol. 12, no. 5, pp. 1187–1196, Sep. 2019, ISSN: 18764754. DOI: 10.1016/j.brs.2019.04.013.

[27] *FAQ: What is phase lag and what effect does it have on DC motors?* [Online]. Available: https://www.motioncontroltips.com/faq-what-is-phase-lag-and-what-effect-does-it-have-on-dc-motors/.

[28] G. B. Saturnino, K. H. Madsen, and A. Thielscher, "Optimizing the Electric Field Strength in Multiple Targets for Multichannel Transcranial Electric Stimulation," *bioRxiv*, p. 2020.05.27.118422, May 2020. DOI: 10.1101/2020.05.27.118422. [Online]. Available: https://www.biorxiv.org/content/10.1101/2020.05.27.118422v1%20https://www.biorxiv.org/content/10.1101/2020.05.27.118422v1.abstract.

[29] I. Alekseichuk, M. Wischnewski, and A. Opitz, "A minimum effective dose for (transcranial) alternating current stimulation," *Brain Stimulation*, vol. 15, pp. 1221–1222, 2022. DOI: 10.1016/j.brs.2022.08.018. [Online]. Available: https://doi.org/10.1016/j.brs.2022.08.018..

[30] J. S. Lee, S. Bestmann, and C. Evans, "A Future of Current Flow Modelling for Transcranial Electrical Stimulation?" *Current Behavioral Neuroscience Reports*, vol. 8, no. 4, pp. 150–159, Dec. 2021, ISSN: 21962979. DOI: 10.1007/S40473-021-00238-5/FIGURES/4. [Online]. Available: https://link-springer-com.ezproxy2.utwente.nl/article/10.1007/s40473-021-00238-5.

[31] B. C. Schwab and S. Huertas Penen, "Syllabus - Bioelectromagnetics," University of Twente, Tech. Rep., 2021, pp. 3–18.

[32] SimNIBS Developers, *FAQ — SimNIBS 3.2.6 documentation*. [Online]. Available: https://simnibs.github.io/simnibs/build/html/faq.html.

[33] G. B. Saturnino, K. H. Madsen, H. R. Siebner, and A. Thielscher, "How to target inter-regional phase synchronization with dual-site Transcranial Alternating Current Stimulation," *NeuroImage*, vol. 163, pp. 68–80, Dec. 2017, ISSN: 1053-8119. DOI: 10.1016/J.NEUROIMAGE.2017.09.024.

[34] R. M. Reinhart, J. D. Cosman, K. Fukuda, and G. F. Woodman, "Using transcranial direct-current stimulation (tDCS) to understand cognitive processing," *Attention, perception & psychophysics*, vol. 79, no. 1, p. 3, Jan. 2017, ISSN: 1943393X. DOI: 10.3758/S13414-016-1224-2. [Online]. Available: /pmc/articles/PMC5539401/%20/pmc/articles/PMC5539401/?report=abstract%20https://www.ncbi.nlm.nih.gov/pmc/articles/PMC5539401/.

[35] D. L. Li, W. T. Rath, H. L. Journee, R. J. Sclabassi, and M. Sun, "Finite element analysis of transcranial electrical stimulation for intraoperative monitoring," *Proceedings of the IEEE Annual Northeast Bioengineering Conference, NEBEC*, pp. 96–97, 2005, ISSN: 1071121X. DOI: 10.1109/NEBC.2005.1431942.

[36] S. Makarov, M. Horner, and G. Noetscher, *Brain and Human Body Modeling*. Springer International Publishing, 2019. DOI: 10.1007/978-3-030-21293-3.

[37] G. B. Saturnino, K. H. Madsen, and A. Thielscher, "Electric field simulations for transcranial brain stimulation using FEM: an efficient implementation and error analysis," *Journal of Neural Engineering*, vol. 16, no. 6, p. 066 032, Nov. 2019, ISSN: 1741-2552. DOI: 10.1088/1741-2552/AB41BA. [Online]. Available: https://iopscience.iop.org/article/10.1088/1741-2552/ab41ba%20https://iopscience.iop.org/article/10.1088/1741-2552/ab41ba/meta.

[38] A. Thielscher, A. Antunes, and G. B. Saturnino, "Field modeling for transcranial magnetic stimulation: A useful tool to understand the physiological effects of TMS?" *Proceedings of the Annual International Conference of the IEEE Engineering in Medicine and Biology Society, EMBS*, vol. 2015-November, pp. 222–225, Nov. 2015, ISSN: 1557170X. DOI: 10.1109/EMBC.2015.7318340.

[39] V. Fonov, A. C. Evans, K. Botteron, C. R. Almli, R. C. McKinstry, and D. L. Collins, "Unbiased average age-appropriate atlases for pediatric studies," *NeuroImage*, vol. 54, no. 1, pp. 313–327, Jan. 2011, ISSN: 10538119. DOI: 10.1016/J.NEUROIMAGE.2010.07.033.

[40] V. Fonov, A. Evans, R. McKinstry, C. Almli, and D. Collins, "Unbiased nonlinear average age-appropriate brain templates from birth to adulthood," *NeuroImage*, vol. 47, S102, Jul. 2009, ISSN: 10538119. DOI: 10.1016/S1053-8119(09)70884-5.

[41] T. L. Rich and B. T. Gillick, "Electrode Placement in Transcranial Direct Current Stimulation—How Reliable Is the Determination of C3/C4?" *Brain Sciences*, vol. 9, no. 3, Mar. 2019, ISSN: 20763425. DOI: 10.3390/BRAINSCI9030069. [Online]. Available: /pmc/articles/PMC6468365/%20/pmc/articles/PMC6468365/?report=abstract%20https://www.ncbi.nlm.nih.gov/pmc/articles/PMC6468365/.

[42] M. A. Mayka, D. M. Corcos, S. E. Leurgans, and D. E. Vaillancourt, "Three-dimensional locations and boundaries of motor and premotor cortices as defined by functional brain imaging: A meta-analysis," *NeuroImage*, vol. 31, no. 4, p. 1453, Jul. 2006, ISSN: 10538119. DOI: 10.1016/J.NEUROIMAGE.2006.02.004. [Online]. Available: /pmc/articles/PMC2034289/%20/pmc/articles/PMC2034289/?report=abstract%20https://www.ncbi.nlm.nih.gov/pmc/articles/PMC2034289/.

[43] D. Purves, G. Augustine, D. Fitzpatrick, W. C. Hall, A.-S. LaMantia, and L. E. White, *Neuroscience*. Oxford : Oxford University Press, 2018, p. 402, ISBN: 9781605357416.

[44] A. W. Toga and P. M. Thompson, "Mapping brain asymmetry," *Nature Reviews Neuroscience 2003 4:1*, vol. 4, no. 1, pp. 37–48, 2003, ISSN: 1471-0048. DOI: 10.1038/nrn1009. [Online]. Available: https://www.nature.com/articles/nrn1009.

[45] Y. Mizutani-Tiebel *et al.*, "Differences in electric field strength between clinical and non-clinical populations induced by prefrontal tDCS: A cross-diagnostic, individual MRI-based modeling study," *NeuroImage : Clinical*, vol. 34, p. 103 011, Jan. 2022, ISSN: 22131582. DOI: 10.1016/J.NICL.2022.103011. [Online]. Available: /pmc/articles/PMC9125784/%20/pmc/articles/PMC9125784/?report=abstract%20https://www.ncbi.nlm.nih.gov/pmc/articles/PMC9125784/.

Appendix A - Results of simulation of different ring electrode montages

Simulation - Ring electrode montage (20, 30, 75)

For the simulation with the electrodes where $D_{circle} = 20mm$ mm, $D_{ring-in} = 30$ mm, and $D_{ring-out} = 75$ mm, the maximum of the electric field strength with the two electrodes in both in-phase and anti-phase is approximately 0.06 V/m (see Figures 26 and 27). For the in-phase simulation, the maximum electric field strength is 5.59×10^{-2} V/m in the left hemisphere and 4.67×10^{-2} V/m in the right hemisphere. For the anti-phase simulation, the maximum electric field strength is 5.83×10^{-2} V/m in the left hemisphere and 4.14×10^{-2} V/m in the right hemisphere. The focality for the in-phase stimulation is 5.54×10^3 mm^3 and 4.89×10^3 mm^3 for the anti-phase stimulation. In comparison to the other electrode sizes, this electrode gives a relatively low electric field strength and a relatively high field focality (see Tables 3 and 4).

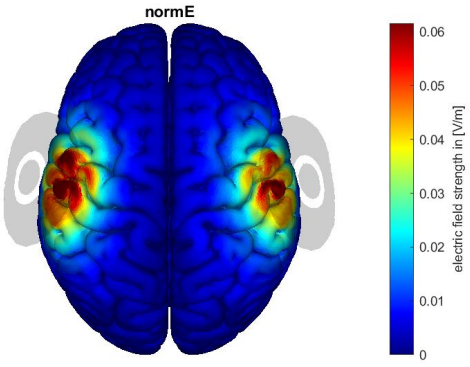

Figure 26: The distribution of the E-field when there is a phase-lag between cortices of 0, with $D_{circular} = 20$ mm, $D_{inner} = 30$ mm, and $D_{outer} = 75$ mm. The maximum electric field strength is approximately 0.06 V/m.

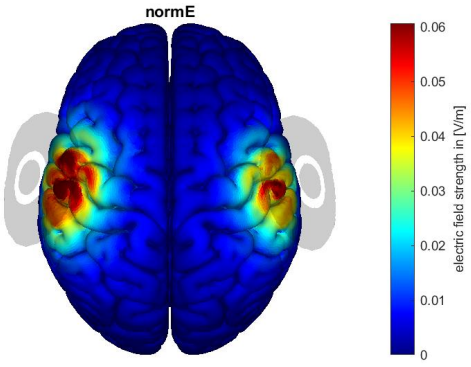

Figure 27: The distribution of the E-field when there is a phase-lag between cortices of π, with $D_{circular} = 20$ mm, $D_{inner} = 30$ mm, and $D_{outer} = 75$ mm. The maximum electric field strength is approximately 0.06 V/m.

Simulation - Ring electrode montage (34, 70, 100)

For the simulation with the electrodes where $D_{circle} = 34$ mm, $D_{ring-in} = 70$ mm, and $D_{ring-out} = 100$ mm, the maximum of the electric field strength with the two electrodes in both in-phase and anti-phase is approximately 0.06 V/m (see Figures 28 and 29). For the in-phase simulation, the maximum electric field strength is 1.04×10^{-1} V/m in the left hemisphere and 9.49×10^{-2} V/m in the right hemisphere. For the anti-phase simulation, the maximum electric field strength is 1.11×10^{-1} V/m in the left hemisphere and 9.90×10^{-2} V/m in the right hemisphere. The focality for the in-phase stimulation is 1.15×10^4 mm^3 and 1.15×10^4 mm^3 for the anti-phase stimulation. In comparison to the other electrode sizes, this electrode gives a relatively high electric field strength and a relatively low field focality (see Tables 3 and 4).

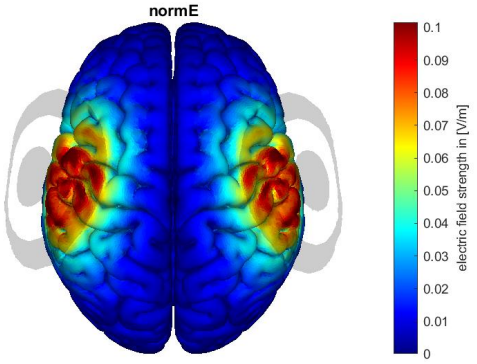

Figure 28: The distribution of the E-field when there is a phase-lag between cortices of 0, with $D_{circular} = 34$ mm, $D_{inner} = 70$ mm, and $D_{outer} = 100$ mm. The maximum electric field strength is approximately 0.1 V/m.

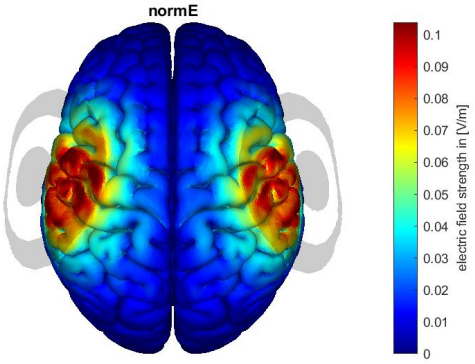

Figure 29: The distribution of the E-field when there is a phase-lag between cortices of π, with $D_{circular} = 34$ mm, $D_{inner} = 70$ mm, and $D_{outer} = 100$ mm. The maximum electric field strength is approximately 0.1 V/m.

Simulation - Ring electrode montage (75, 90, 100)

For the simulation with the electrodes where $D_{circle} = 75$ mm, $D_{ring-in} = 90$ mm, and $D_{ring-out} = 100$ mm, the maximum of the electric field strength with the two electrodes in both in-phase and anti-phase is approximately 0.07 V/m (see Figures 30 and 31). For the in-phase simulation, the maximum electric field strength is 6.12×10^{-2} V/m in the left hemisphere and 5.14×10^{-2} V/m in the right hemisphere. For the anti-phase simulation, the maximum electric field strength is 7.03×10^{-2} V/m in the left hemisphere and 6.40×10^{-2} V/m in the right hemisphere. The focality for the in-phase stimulation is 1.69×10^4 mm^3 and 1.98×10^4 mm^3 for the anti-phase stimulation. In comparison to the other electrode sizes, this electrode gives a relatively low electric field strength and a relatively low field focality (see Tables 3 and 4).

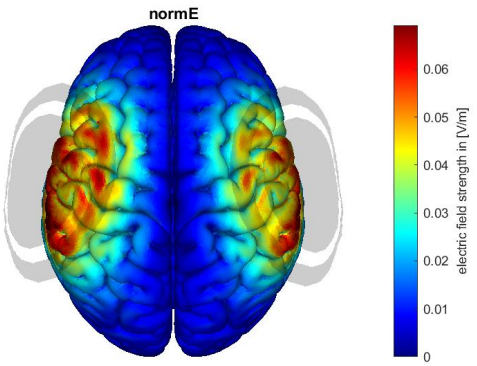

Figure 30: The distribution of the E-field when there is a phase-lag between cortices of 0, with $D_{circular} = 75$ mm, $D_{inner} = 90$ mm, and $D_{outer} = 100$ mm. The maximum electric field strength is approximately 0.07 V/m.

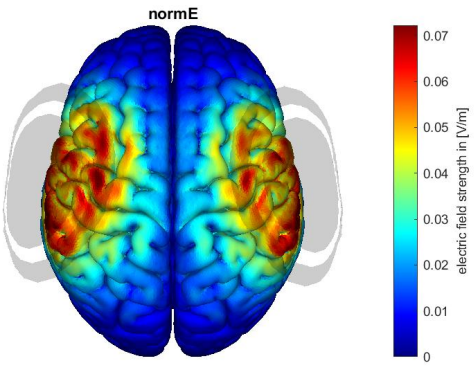

Figure 31: The distribution of the E-field when there is a phase-lag between cortices of π, with $D_{circular} = 75$ mm, $D_{inner} = 90$ mm, and $D_{outer} = 100$ mm. The maximum electric field strength is approximately 0.07 V/m.

Simulation - Ring electrode montage (80, 90, 110)

For the simulation with the electrodes where $D_{circle} = 80$ mm, $D_{ring-in} = 90$ mm, and $D_{ring-out} = 110$ mm, the maximum of the electric field strength with the two electrodes in both in-phase and anti-phase is approximately 0.06 V/m (see Figures 32 and 31). For the in-phase simulation, the maximum

electric field strength is 5.29×10^{-2} V/m in the left hemisphere and 4.24×10^{-2} V/m in the right hemisphere. For the anti-phase simulation, the maximum electric field strength is 6.11×10^{-2} V/m in the left hemisphere and 5.51×10^{-2} V/m in the right hemisphere. The focality for the in-phase stimulation is 1.64×10^4 mm^3 and 1.98×10^4 mm^3 for the anti-phase stimulation. In comparison to the other electrode sizes, this electrode gives a relatively low electric field strength and a relatively low field focality (see Tables 3 and 4).

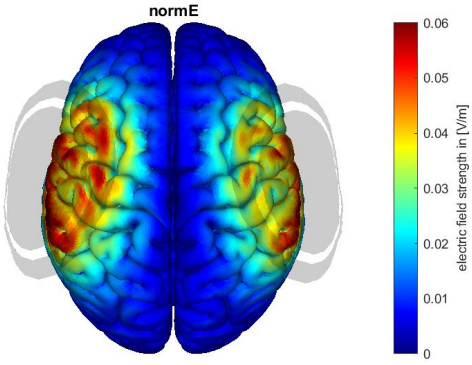

Figure 32: The distribution of the E-field when there is a phase-lag between cortices of 0, with $D_{circular} = 80$ mm, $D_{inner} = 90$ mm, and $D_{outer} = 110$ mm. The maximum electric field strength is approximately 0.06 V/m.

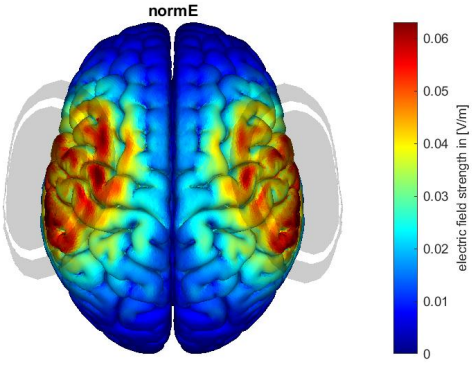

Figure 33: The distribution of the E-field when there is a phase-lag between cortices of π, with $D_{circular} = 80$ mm, $D_{inner} = 90$ mm, and $D_{outer} = 110$ mm. The maximum electric field strength is approximately 0.06 V/m.

Appendix B - Difference in electric field strength for phase-lag value simulations

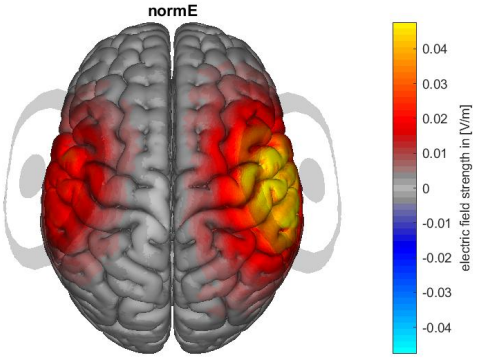

Figure 34: The difference in electric field strength between the simulation for $\phi = 0$ and $\phi = \frac{1}{2}\pi$. The current values for the electrodes with a phase-lag of $\phi = \frac{1}{2}\pi$ are the values at t = 0.13 s. The maximum of the electric field difference is approximately 0.045 V/m.

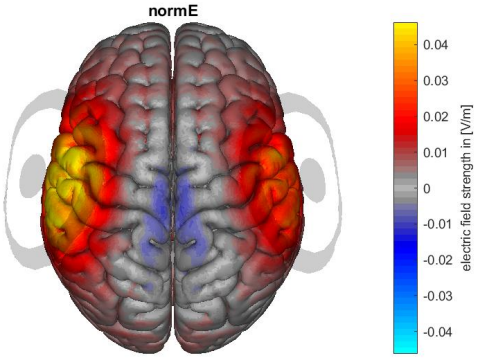

Figure 35: The difference in electric field strength between the simulation for $\phi = 0$ and $\phi = \frac{3}{2}\pi$. The current values for the electrodes with a phase-lag of $\phi = \frac{3}{2}\pi$ are the values at t = 0.08 s. The maximum of the electric field difference is approximately 0.05 V/m.

Appendix C - The direction of the electric field: additional figures

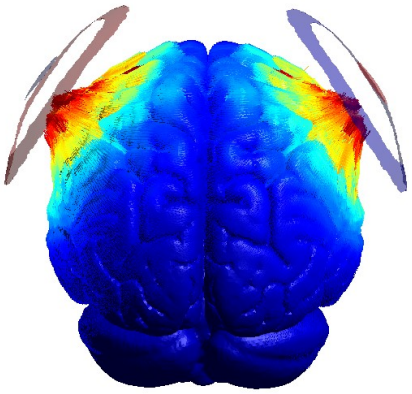

Figure 36: A figure of the simulation where the direction of the electric field is visible. The phase-lag value for the simulation is $\phi = \pi$. The electric field is perpendicular to the cortex in areas where the electric field strength is high (see the dark-red areas in the figure). The electric field gradually changes to be more parallel to the cortex in areas where the electric field strength is lower (see the green/blue areas).

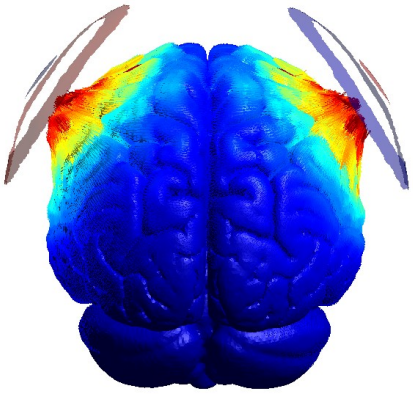

Figure 37: A figure of the simulation where the direction of the electric field is visible. The phase-lag value for the simulation is $\phi = \frac{1}{2}\pi$. The current value is taken at t = 0.0185 s. The electric field is perpendicular to the cortex in areas where the electric field strength is high (see the dark-red areas in the figure). The electric field gradually changes to be more parallel to the cortex in areas where the electric field strength is lower (see the green/blue areas).

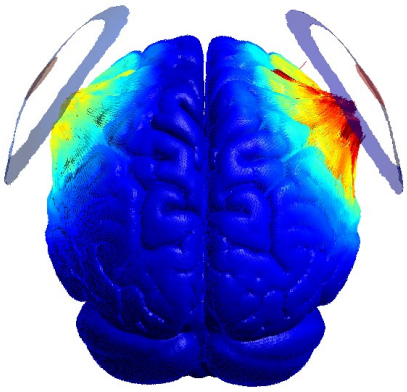

Figure 38: A figure of the simulation where the direction of the electric field is visible. The phase-lag value for the simulation is $\phi = \frac{3}{2}\pi$. The currentn value is taken at t = 0.017 s. The electric field is perpendicular to the cortex in areas where the electric field strength is high (see the dark-red areas in the figure). The electric field gradually changes to be more parallel to the cortex in areas where the electric field strength is lower (see the green/blue areas).

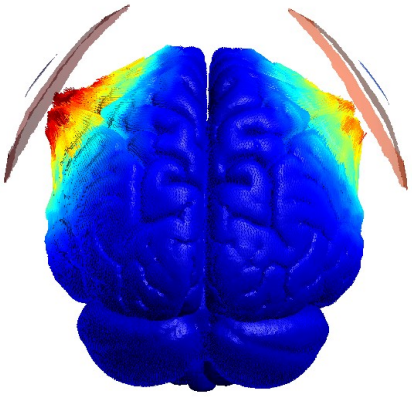

Figure 39: A figure of the simulation where the direction of the electric field is visible. The phase-lag value for the simulation is $\phi = \frac{1}{2}\pi$. The current value is taken at t = 0.13 s. The electric field is perpendicular to the cortex in areas where the electric field strength is high (see the dark-red areas in the figure). The electric field gradually changes to be more parallel to the cortex in areas where the electric field strength is lower (see the green/blue areas).

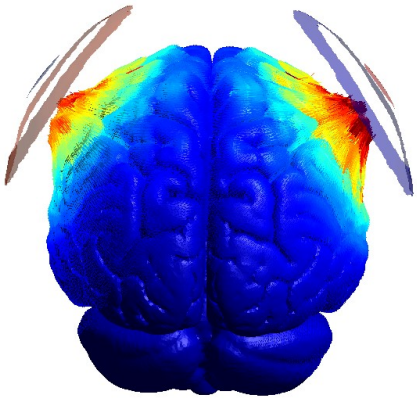

Figure 40: A figure of the simulation where the direction of the electric field is visible. The phase-lag value for the simulation is $\phi = \frac{3}{2}$. The current value is taken at t = 0.08 s The electric field is perpendicular to the cortex in areas where the electric field strength is high (see the dark-red areas in the figure). The electric field gradually changes to be more parallel to the cortex in areas where the electric field strength is lower (see the green/blue areas).